



VCU

Virginia Commonwealth University
VCU Scholars Compass

Theses and Dissertations

Graduate School

2002

Computational Simulations Concerning Unsteadiness Attenuation in Axial Turbines

Robert R. Croft

Follow this and additional works at: <https://scholarscompass.vcu.edu/etd>



Part of the [Mechanical Engineering Commons](#)

© The Author

Downloaded from

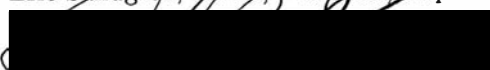
<https://scholarscompass.vcu.edu/etd/4448>

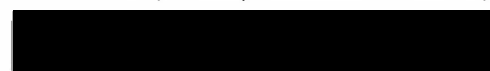
This Thesis is brought to you for free and open access by the Graduate School at VCU Scholars Compass. It has been accepted for inclusion in Theses and Dissertations by an authorized administrator of VCU Scholars Compass. For more information, please contact libcompass@vcu.edu.


School of Engineering
Virginia Commonwealth University

This is to certify that the thesis prepared by Robert R. Croft entitled Computational Simulations Concerning Unsteadiness Attenuation in Axial Turbines has been approved by his committee as satisfactory completion of the thesis requirement for the degree of Master of Science.


Eric Sandgren, Ph.D., Professor, Department of Mechanical Engineering


Daniel Cook, Ph.D., Assistant Professor, Department of Mechanical Engineering


Timothy Cameron, Ph.D., Associate Professor, Department of Mechanical Engineering


Gerald Miller, Ph.D., Chair, Department of Biomedical Engineering


Robert J. Mattauch School of Engineering


F. Douglas Boudinot, Ph.D., Dean, School of Graduate Studies

8/15/02
Date

**Computational Simulations Concerning Unsteadiness Attenuation in
Axial Turbines**

A thesis submitted in partial fulfillment of the requirements for the degree of
Master of Science at Virginia Commonwealth University.

By
Robert R. Croft, Bachelor of Science
Virginia Commonwealth University
2000

Director: Eric Sandgren, Professor, Department of Mechanical Engineering, Ph.D.

Virginia Commonwealth University
Richmond, Virginia
August, 2002

ACKNOWLEDGMENT

I first wish to thank Dr. Daniel J. Dorney, for the inspiration to continue the undergraduate process and to embark on the graduate trek. Were it not for him I am certain that I would have chosen another avenue of study. Secondly, I would like to extend my gratitude to the faculty of the Mechanical Engineering Department of the School of Engineering at Virginia Commonwealth University. Never can I recall not being able to take a problem to them, nor having anything less than total attention when I did so. Lastly, to my parents, Bob and Debra, brothers Thomas and Jeremiah, wife Angela and son Zachery, their love and endurance has often served as my foundation, ambition, and fountain of youth.

TABLE OF CONTENTS

| | |
|---|------|
| LIST OF FIGURES | v |
| LIST OF SYMBOLS | viii |
| ABSTRACT | xi |
| 1 Introduction | 1 |
| 1.1 Hot Streaks | 2 |
| 1.1.1 NASA CERTS | 4 |
| 1.1.2 LSRR | 6 |
| 1.2 Clocking | 9 |
| 1.3 Previous Results | 13 |
| 1.4 Current Investigation | 15 |
| 2 Numerical Integration Procedure | 17 |
| 3 Geometry | 20 |
| 4 Gridding | 22 |
| 5 Boundary Conditions | 25 |
| 6 Hot Streak Results | 28 |
| 7 Hot Streak Grid Resolution Results | 30 |
| 8 Hot Streak Results at Frequencies Less Than Unity | 36 |
| 9 Hot Streak Results at Unity | 40 |
| 10 Clocking Effects on Hot Streak Migration | 44 |
| 11 Embedded Stage Clocking Results | 48 |
| 12 Conclusions | 65 |
| BIBLIOGRAPHY | 67 |

| | |
|-----------|----|
| VITA..... | 70 |
|-----------|----|

LIST OF FIGURES

| Figure | Page |
|--|------|
| 1.1 Kerrebrock-Mikolajczak Effect..... | 3 |
| 1.2 NASA CERTS Configuration..... | 5 |
| 1.3 UTRC LSRR Configuration..... | 7 |
| 4.1 Full Computational Grid - Clocking Case..... | 23 |
| 4.2 Close Up of Nozzle 2 - Nozzle 3 Computational Grid - Clocking Case.... | 24 |
| 7.1 Instantaneous Static Temperature Contours - 0.0 BPF..... | 32 |
| 7.2 Instantaneous Static Temperature Contours - 0.5 BPF..... | 32 |
| 7.3 Time-Averaged Total Temperature - 0.00 BPF - Stator 1 Inlet..... | 33 |
| 7.4 Time-Averaged Total Temperature - 0.50 BPF - Stator 1 Inlet..... | 33 |
| 7.5 Time-Averaged Total Temperature - 0.00 BPF - Rotor 1 Exit..... | 34 |
| 7.6 Time-Averaged Total Temperature - 0.50 BPF - Rotor 1 Exit..... | 34 |
| 7.7 Time-Averaged Total Temperature Surface Profile - 0.00 BPF - Rotor 1 . | 35 |
| 7.8 Time-Averaged Total Temperature Surface Profile - 0.50 BPF - Rotor 1. | 35 |
| 8.1 Time-Averaged Total Temperature - Stator 1 Exit..... | 38 |
| 8.2 Time-Averaged Total Temperature Surface Profile - Rotor 1..... | 38 |
| 8.3 Time-Averaged Total Temperature - Rotor 1 Exit..... | 39 |
| 8.4 Time-Averaged Total Temperature Surface Profile - Stator 2..... | 39 |
| 9.1 Time-Averaged Total Temperature - Stator 1 Inlet - 1.00 BPF..... | 41 |
| 9.2 Time-Averaged Total Temperature - Stator 1 Exit - 1.00 BPF..... | 42 |

| | | |
|-------|--|----|
| 9.3 | Time-Averaged Total Temperature Surface Profile - Rotor 1 - 1.00 BPF. | 42 |
| 9.4 | Time-Averaged Total Temperature - Rotor 1 Exit - 1.00 BPF. | 43 |
| 9.5 | Time-Averaged Total Temperature Surface Profile - Stator 2 - 1.00 BPF. | 43 |
| 10.1 | Time-Averaged Total Temperature - 1.00 BPF - Clocked and Synchronized. | 45 |
| 10.2 | Time-Averaged Total Temperature Surface Profile - Rotor 1 - 1.00 BPF - Clocked and Synchronized..... | 46 |
| 10.3 | Time-Averaged Total Temperature Surface Profile - Stator 2 - 1.00 BPF - Clocked and Synchronized..... | 46 |
| 10.4 | Time-Averaged Total Temperature - Stator 2 Clocked - 0.50 BPF. | 47 |
| 10.5 | Time-Averaged Total Temperature Surface Profile - Stator 2 Clocked - 0.50 BPF. | 47 |
| 11.1 | Full Annulus Instantaneous Mach Contours - High Efficiency..... | 52 |
| 11.2 | Nozzle 2 - Nozzle 3 Instantaneous Mach Contours - High Efficiency..... | 52 |
| 11.3 | Full Annulus Instantaneous Entropy Contours - High Efficiency. | 53 |
| 11.4 | Nozzle 2 - Nozzle 3 Instantaneous Entropy Contours - High Efficiency. .. | 53 |
| 11.5 | Nozzle 2 - Nozzle 3 Time-Averaged Entropy Contours - Low Efficiency. . | 54 |
| 11.6 | Nozzle 2 - Nozzle 3 Time-Avgeraged Entropy Contours - High Efficiency. | 54 |
| 11.7 | Stage Efficiencies. | 55 |
| 11.8 | Vane Losses With Respect to Vane 3 Clocking Position. | 55 |
| 11.9 | Rotor Losses With Respect to Vane 3 Clocking Position..... | 56 |
| 11.10 | Unsteady Pressure Envelopes - Vane 1..... | 56 |
| 11.11 | Unsteady Pressure Envelopes - Vane 2..... | 57 |
| 11.12 | Unsteady Pressure Envelopes - Vane 3..... | 57 |
| 11.13 | Unsteady Pressure Envelopes - Vane 4..... | 58 |
| 11.14 | Maximum and Minimum Unsteady Pressure Envelopes - Vane 2..... | 58 |

| | | |
|-------|--|----|
| 11.15 | Maximum and Minimum Unsteady Pressure Envelopes - Vane 3..... | 59 |
| 11.16 | Maximum and Minimum Unsteady Pressure Histories - Vane 3 Leading Edge. | 59 |
| 11.17 | Unsteady Pressure Envelopes - Rotor 1. | 60 |
| 11.18 | Unsteady Pressure Envelopes - Rotor 2. | 60 |
| 11.19 | Unsteady Pressure Envelopes - Rotor 3. | 61 |
| 11.20 | Unsteady Pressure Envelopes - Rotor 4. | 61 |
| 11.21 | Maximum and Minimum Unsteady Pressure Envelopes - Rotor 2..... | 62 |
| 11.22 | Maximum and Minimum Unsteady Pressure Envelopes - Rotor 3..... | 62 |
| 11.23 | Time-Averaged Absolute Exit Flow Angle - Nozzle 1..... | 63 |
| 11.24 | Time-Averaged Absolute Exit Flow Angle - Nozzle 2..... | 63 |
| 11.25 | Time-Averaged Absolute Exit Flow Angle - Nozzle 3..... | 64 |
| 11.26 | Time-Averaged Absolute Exit Flow Angle - Nozzle 4..... | 64 |

LIST OF SYMBOLS

Standard Nomenclature

| | |
|--------|------------------------------------|
| a | Speed of sound |
| rpm | Revolutions per minute |
| u, v | X and Y velocity directions |
| BPF | Blade passing frequency |
| C_p | Specific heat at constant pressure |
| C_v | Specific heat at constant volume |
| $L.E.$ | Leading edge |
| M | Mach number |
| P | Pressure |
| $P.S.$ | Pressure surface |
| P_r | Prandtl number |
| Re | Reynolds number |
| S | Actual surface area |
| $S.S.$ | Suction surface |
| T | Temperature |
| U | Rotor rotational Velocity |
| V | Absolute reference frame velocity |
| W | Relative reference frame velocity |

Greek letter symbols

| | |
|----------|--|
| ρ | Density |
| α | Absolute angle of attack |
| β | Relative angle of attack |
| γ | Ratio of specific heats |
| ϕ | Flow Coefficient |
| μ | Dynamic viscosity |
| η | Efficiency |
| Δ | Standard difference ($a_1 - a_0$) = Δa |
| Ω | Angular Velocity |

Subscripts

| | |
|----------|-----------------------------|
| ∞ | Free stream quantity |
| amp | Amplitude |
| $exit$ | Rig exit |
| s | Static |
| t | Total |
| tt | Total-to-total |
| $wetted$ | Planar surface area |
| HS | Hot streak |
| L | Laminar |
| T | Turbulent |
| 0 | Vane 1 inlet |
| 1 | Vane 1 exit / Rotor 1 inlet |
| 2 | Rotor 1 exit / Vane 2 inlet |

| | |
|---|-----------------------------|
| 3 | Vane 2 exit / Rotor 2 inlet |
| 4 | Rotor 2 exit / Vane 3 inlet |
| 5 | Vane 3 exit / Rotor 3 inlet |
| 6 | Rotor 3 exit / Vane 4 inlet |
| 7 | Vane 4 exit / Rotor 4 inlet |
| 8 | Rotor 4 exit |

ABSTRACT

Computational Simulations Concerning Unsteadiness Attenuation in Axial Turbines.

By Robert R. Croft, Master of Science

A thesis submitted in partial fulfillment of the requirements for the degree of
Master of Science at Virginia Commonwealth University.

Virginia Commonwealth University, 2002

Major Director: Eric Sandgren, Professor, Department of Mechanical Engineering,
Ph.D.

Axial turbomachines have inherently unstable flow fields due to the interaction between rotating and nonrotating blade rows. In addition, combustor instabilities add considerable stress on the blading via the introduction of localized radial and/or circumferential temperature discontinuities known as hot streaks. To alleviate the losses due to nonconformities within the turbine a computational effort has been undertaken investigating the effects of clocking an imbedded stage in a multi-stage axial turbine and a separate study considering the effects of an imposed temporally oscillating hot streak within a $1\frac{1}{2}$ stage turbine. Time-dependent hot streak results

show little relation of rotor surface heating to hot streak frequency (non-dimensional) for hot streak frequencies less than unity. The general trend for stator 2 is observed to be as hot streak frequency increases stator 2 observes a decreasing trend in surface heating for frequencies less than unity. At unity rotor surface heating is minimized and stator 2 surface heating is maximized, if the rotor is properly phased (180°) with the hot streak. When the hot streak is in phase with the rotor a rotor maximum surface temperature is observed and the stator 2 is at a minimum. Multi-stage clocking shows a periodic effect on loss and efficiency for the clocked airfoils and the rotor between. Loss and efficiency in the current study are observed to vary inversely to one another with high vane loss corresponding to higher efficiency in the vane rows, while high loss in the vane corresponds to low losses of greater magnitude in the rotor row.

CHAPTER 1 Introduction

Axial turbines have inherently unsteady flow fields. This is a result of wake/wake interaction, wake/airfoil interaction, potential flows (viscous and inviscid effects), and combustor exit anomalies, and as a direct result of the latter, complex cooling flow patterns. It has been shown that entropy has a stacking effect as axial distance increases and as blade rows are increased, due to added unsteady interactions. Consequently efficiency, durability, and reliability suffer. Two ways of managing and abating this unsteadiness are a) hot streak management and b) airfoil clocking.

Hot streaks are defined as localized temperature spikes within the combustor exit flow field. Typically, this intrusion is modeled as a circular total temperature distortion, holding total and static pressure constant to the free stream flow. This is due to experiments of Roback and Dring [4, 5]. Introduction of the hot streak is limited to two (2) pitchwise positions, midpassage and directly impacting the first-stage stator leading edge. This is because these cases represent (respectively) the least and greatest influence of the stator on the hot streak migration (*i.e.* hot streak impaction on the stator forces convection of the hot fluid across the stator surfaces whereas introduction at midpassage allows for uninhibited flow through the passage, varying only due to a reduction in area through the throat). These positions can also be interpreted as the worst and best with respect to rotor thermal loading. As can be inferred, impaction of the hot streak on the first-stage stator decreases the inlet temperature to the first-stage rotor through convection and wake mixing, whereas

if the hot streak is allowed to move unabated (non-impacting) through the stator passage, the rotor observes the entirety of the hot streak, and having been reduced in area by passing through the nozzle throat, localized temperatures are more intense. Clocking or “indexing” refers to the relative positioning of adjacent stator (or rotor) airfoils in order to adequately receive and convect the upstream airfoil wake. Entropy is generally used to trace areas of high loss, since high entropy corresponds to high loss, however, vorticity is a good indicator of loss also. Mach number is also a good indicator of areas of high loss due to shocks. Often clocking studies are conducted in conjunction with inter-blade-row gap studies since modern turbomachine blades are cambered as to receive flow from the upstream blade row. Similar to hot streak studies, when the wake is forced to impact the leading edge of the downstream blade row, efficiency is observed to be at a local maximum, the opposite is true for wake convection through midpassage. This is directly related to work extraction by the rotor as proper wake passing leads to higher work extraction and consequently higher stage efficiencies.

1.1 Hot Streaks

Modern combustor exit temperatures can locally exceed the rated metal temperatures by as much as 50-100°F (28-55°C). As a point of reference, it has been shown that a 100°F difference in temperature can reduce the blade life by a full order of magnitude. Experimental data taken from gas turbine combustors have confirmed the existence of these large temperature gradients in both the radial and circumferential directions [1, 2], which stem from the interaction of combustor core flows, combustor bypass flows, and cooling flows. The nominal range of hot streak temperature is 1.1-1.6 times that of the free stream, however, it has been observed that the hot streak flow can reach more than twice that found in the free stream flows.

Advanced cooling schemes are employed to countermand the influence of hot streaks. This cooler fluid flow is most often applied like a film to the blade surface creating a sacrificial boundary layer to prevent the blade burnout. Cooling flows can also accumulate downstream of the blade row, resulting in a 'cold streak' or phantom cooling as a side effect to this preventive measure. The interaction of hot/cold streak results in greater thermal fatigue to the influenced blade rows. The colder fluid is more apt to impact on the suction surface of the downstream blade row, whereas the hotter fluid impinges on the pressure surface. This is due primarily to velocity differences in the flows in comparison to free stream flows known as the Kerrebrock-Mikolajczak effect [3].

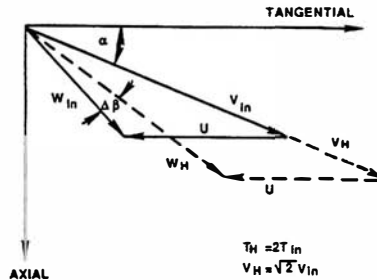


Figure 1.1: Kerrebrock-Mikolajczak Effect.

where the subscript 'in' represents initial or design flow and the subscript 'H' represents hot gas flow.

As seen in Fig. 1.1, the hotter fluid has a greater total velocity in comparison to the free stream where the colder is the converse. In the rotor, or relative reference frame, this total velocity difference correlates to an increase in the relative flow angle β , entering the rotor passage. Due to this it is seen how the hotter fluid exiting the

stator row is more apt to impact on the rotor pressure surface, whereas the colder fluid is more inclined to propagate towards the passage, or suction surface of the following rotor blade. Since the two flows do not exhibit the same flow characteristics (i.e. incidence and velocity profiles) it is not feasible to use one to countermand the effects of the other [4, 5]. It is imperative that true hot/cold streak interaction be understood in order to accurately design turbine blading and passages that will achieve optimal efficiency and durability in the presence of these anomalies.

1.1.1 NASA CERTS

Researchers at the former NASA Lewis Research Center performed some of the earliest experimental testing. Their testing centered on the Combustor Exit Radial Temperature Simulator (CERTS). The goal of these experiments was to analyze the effects of combustor exit radial temperature discontinuities on axial turbine performance. The test rig (Fig. 1.2) is a 0.767 scale model of the first stage of a two-stage warm core turbine designed for a high bypass ratio engine. The stators were untwisted (of constant cross section) and designed for 75° flow turning. The blades had reasonable height and the rotor was designed to accept the stator wake with zero or small negative incidence. The CERTS air is pumped in through circumferential slots in the hub and tip endwalls upstream of the stator. This simulation was performed both with and without the CERTS air on; temperature profiles for these hot streak simulations showed that the highest temperature coefficient measured for the case without CERTS is considerably lower than the case with CERTS. The difference between the two cases was 0.6. This results from the improper flow interaction due to incidence effects from the higher velocity of the hotter flow contributions.

Additionally, there have been simulations performed using the CERTS geometry, the first of which was as part of an experimental study by Schwab *et al.* [6]. This was

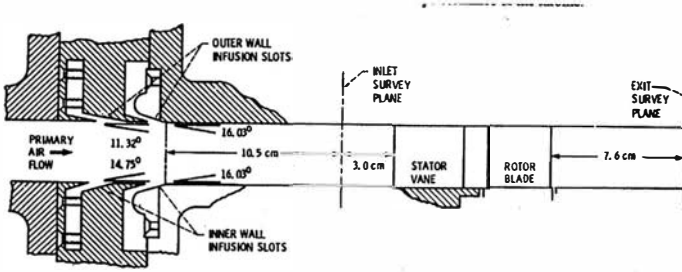


Figure 1.2: NASA CERTS Configuration.

performed using an inviscid flow solver for Euler equations, and showed a chordwise progression of temperature on both the rotor and stator airfoils for the pressure and suction surfaces. This was attributed to secondary flows. A second simulation was later performed by Dorney and Schwab [7] using two- and three-dimensional, viscous and inviscid modeling. Both simulations agreed with the experimental testing, however, the three-dimensional simulation had the strongest correlation to the experimental tests showing a redistribution of the hot streak to the pressure surface of the airfoils, as well as strong underturning of the flow, both of which was attributed to secondary flows. Tip clearance was also discovered to have considerable impact on the rotor flow angle from 60% to 100% span.

Dorney and Gundy-Burlet [8] performed a study concerning hot streak shape in relation to rotor surface heating. The study included multiple sizes of circular and elliptical hot streaks using a temperature ratio of $\frac{T_{HS}}{T_{\infty}} = 1.2$. Results from this study showed that larger hot streak surface areas allowed for greater secondary flow interaction creating more increased temperature regions. Elliptical hot streaks were found to dissipate more rapidly with the free stream due to the increased surface area in contact with the cooler core flow. Rotor average surface temperature is minimally

effected by hot streak shape or temperature ratio. Blade Surface temperature flux is more than linearly effected hot streak shape for a constant temperature ratio.

1.1.2 LSRR

There have been a considerable number of experiments performed on the Large Scale Rotating Rig (LSRR) at The United Research Technologies (UTRC). The LSRR (Fig. 1.3) is a low-speed, large-scale, rotating wind tunnel facility that is set up to model the flow through modern axial turbomachines. The primary concerns in the construction of this facility was to provide:

- A flow region large enough so as to provide a high resolution for three-dimensional flows
- Have a pragmatic variety of configurations that could be accommodated
- Allow relative frame measurements to be made directly

A more complete description of this geometry can be found in Chapter 3, and in Butler *et al.* [1].

Gundy-Burlet and Dorney [9] used a three-dimensional analytical model to show that the pressure surface boasts a local hot spot from the impact of an introduced temperature distortion due to the slower relative velocity on the surface, which results in a decreased rate of convection of the hot streak fluid across the airfoil. Instead of linear convection as would normally occur just from the path of the flow, the hot streak radially convects along the pressure surface of the airfoil until it reaches the four physical boundaries. Once it reaches the leading edge it wraps around and is then convected along the suction surface at a higher velocity resulting in very little additional blade heating. At the trailing edge, hub, and endwall the flow ends and is

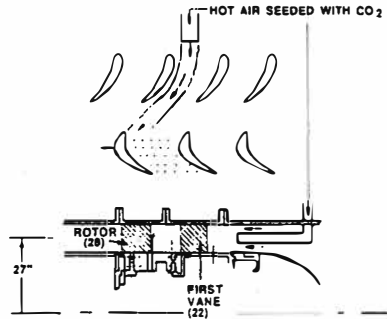


Figure 1.3: UTRC LSRR Configuration.

convected by the free-stream. Additionally, it was observed that one way to alleviate the excess thermal loading of the rotor blading through clocking the hot streak in reference to the first-stage stator. In doing this the hot streak is aligned such that it impinges directly in the leading edge of the airfoil, forcing convection along both sides of the stator. This in turn forces additional mixing of the hot gas with the vane wake and free stream fluid in the interblade region. When this mixing occurs the thermal load to the rotor is considerably lower since the hot streak has been made to dissipate in the free stream.

Takahashi *et al.* [10] and Takahashi and Ni [11, 12] performed a similar study including various blade counts. It was determined that, two-dimensional simulations were not adequate to correctly model the complex flows of a three-dimensional hot streak such as that in the rig primarily due to secondary flows and their impact on airfoil temperature profile in the presence of hot streaks. However, a two-dimensional code was found adequate when modeling a two-dimensional (planar) hot streak. Clocking the hot streak was also determined to have a strong effect on the rotor surface temperatures, decreasing the overall surface profiles by approximately 33%. Rotor

secondary flow vortices were also shown to continue into the second stator passage transporting flows from the suction surfaces radially to the endwalls. Temperature results for stator 2 were observed to lack segregation, contradicting the findings of Dorney *et al.* [13] where the second stator was shown to exhibit the same characteristic heating as the rotor.

Hot streaks can also have significant effects on the secondary flow and endwall temperatures [14, 15]. This is due to the radial heating and buoyancy forces related to the hot streak flow having a differing density than that of the free stream [16]. The flow, less rapidly convected by the relatively low pressure side velocity, cedes a considerably higher overall temperature profile to the surface. This in turn begets a greater endwall temperature from the radial convection of the fluid, and a lower localized density. The migration of hot streaks and the heating of rotor surfaces are primarily controlled by two flow contributions, rotor passage secondary flows and hot and cold gas separation as caused by the difference in velocity profiles and thereby in adjacent blade incidence [11, 17].

A more recent study by Gundy-Burlet and Dorney [18] investigates the effects of varying the radial introduction of the hot streak in addition to circumferential variations. Positions that were of interest were 20, 40, and 60% span, studied with introduction at mid-passage and directly impacting the first-stage stator. Impinging the hot streak on the first-stage vane creates a large, though temporally stable thermal load, which should be easily rectified by blade cooling, and since the flow is nearly constant in time, additional cooling measures used to rectify the new loading can be used in an efficient manner. Mid-passage, mid-span hot streak introduction reduces secondary flow interaction but greatly increases the loading on the pressure surface of the rotor due to the hot gas passing relatively uninhibited to the rotor. The rotor and second-stage stator become desensitized to hot streak placement when impacted

on the first-stage stator. Tip region introduction instigates higher time-averaged temperatures to a region that is already prone to blade-burning and failure.

1.2 Clocking

Clocking, or ‘indexing’ refers to adjusting the relative circumferential position of adjacent stator (or rotor) rows with respect to the upstream blade row. Driving forces behind the movement to better understand the effects of clocking stem from the inherent unsteadiness already present in turbomachinery. Wake/airfoil and wake/wake interactions, being the greatest sources of unsteadiness, need to be understood to properly design efficient turbomachines. With the current trend of decreasing compressor and turbine size (and consequently axial gapping) and more aggressive flow turning, clocking has received considerable exposure in the past two decades, including turbine applications. It has been shown that clocking airfoils can increase efficiency and reduce unsteadiness in multi-stage turbomachines. Conversely, if left unmanaged, wake patterns from upstream rotor rows can result in flow fields that are potentially more degrading to downstream blade rows [19].

One of the earliest investigations of wake/airfoil interaction was performed by Kerrebrock and Mikolajczak [3], producing a wake transport theory to explain the effects of rotor wake passing through intra-stator regions. The resulting development was the Kerrebrock-Mikolajczak effect (Fig. 1.1), which became the basis for hot streak theory as shown previously. However, in the scope of clocking it provides a means of definition for wake passing between blade rows. Assuming an ideal gas, and defining entropy as in Eqn. 1.1, it is seen that pressure loss can be traced through the entropy associated with the wakes. Giles [20] used a computational fluid dynamics (CFD) flow code, UNSFLO, to predict unsteady wake/rotor interactions. Entropy flow fields from his study showed higher entropy lines spreading out on the pressure surface and

lower entropy contours spreading out on the suction surface of the airfoil, showing agreement to the Kerrebrock-Mikolajczak effect.

$$\Delta s = C_p \cdot \ln\left(\frac{T_2}{T_1}\right) + R \cdot \ln\left(\frac{P_2}{P_1}\right) \quad (1.1)$$

Gundy-Burlet and Dorney [21] investigated the effects of both clocking and inter-blade gap on efficiency and unsteadiness in a $2\frac{1}{2}$ stage compressor with an inlet guide vane (IGV), by varying the second stator axial gap (moving stator 2 relative to rotor 2) and circumferential positioning. Results from this study showed that efficiency varied positively as axial gap is increased and when the first-stage stator wake convected along the pressure side of stator 2. It was also observed that efficiency can vary by as much as a point with proper clocking. Maximum efficiency for the three axial gaps of interest in this study (20, 35 and 50%) showed a maximum at the same circumferential position indicating that the airfoil was not cambered to accept the rotor wake.

Saren *et al.* [22] and Dorney *et al.* [23] performed numerical and experimental simulations on a $1\frac{1}{2}$ stage high speed compressor with nearly equal blade counts (34-35-34). In both studies, clocking of the IGV and stator were examined. Saren *et al.* [22] reports the experimental portion of these studies and suggested that decreasing axial rotor/stator gap strengthens mid-span clocking effects, while exhibiting little effect on endwall regions. Efficiency was observed to vary by half pitch from minimum-to-maximum values, showing a more periodic effect than was observed in Gundy-Burlet and Dorney [21]. This could be attributed to the addition of a second stage to the compressor, and in so doing additional wake/wake and wake/airfoil interactions to the clocked row. The scaled pressure ratio was shown to have greater magnitude in the mid-span region corresponding to the strengthened clocking effects and produc-

ing larger endwall effects. Experimental changes in efficiency were on the order of 1.0% for the larger axial gap and 1.4% for the smaller. Numerical results for this study were for scaled blade counts (1-1-1) and presented similar results depicting a -0.10 point change in efficiency from smaller to larger axial gap, maximum change in efficiency for both gaps was approximately 1.0%. Pressure ratio was shown to correspond directly to efficiency. Both cases indicated that decreasing axial gap placed greater unsteady loads on the rotor. Combined effects of IGV and stator clocking show upstream interactions (potential) effects on the rotor.

Using true blade counts (full annulus) Dorney *et al* [23] varied flow parameters to off design points (stall, choke, and optimum). Clocking was observed to be most significant near the design point, slightly less at near stall, and least significant at choke. Stage total pressure ratio and efficiency as a function of clocking was shown to be minimally affected by operating condition (*i.e.*, for all cases, stage pressure ratio and efficiency were nearly in phase) further supporting the results from Saren *et al* [22]. Flow turning (β) was shown to correlate directly to efficiency and loss in the rotor and inversely in the stator. Hence, performance increases due to stator clocking were associated with higher flow turning from the rotor and lower stator losses. Full annulus efficiency was observed to be lower than in the equal blade count simulations [22], this is consistent with a later study by Dorney *et al* [24].

Clocking in turbines has also received considerable attention in the past few years. Dorney and Sharma [25] observed an offset of one-half stator pitch between maximum and minimum efficiencies, similar to previous compressor clocking studies [21, 22, 23]. The magnitude of unsteadiness was also shown to directly relate to efficiency as larger measured values of unsteadiness (taken near the leading edge locations on the clocked vane) correlate to higher stage efficiencies.

Cizmas and Dorney [26] performed a complex study extending clocking to both

rotor and stator rows in a three-stage turbine, using scaled blade counts. Maximum efficiency for stator clocking occurred when first-stage stator wakes impinged the leading edge of the second-stage stator, slightly shifted to the pressure surface, as was shown by Gundy-Burlet and Dorney [21]. Rotor clocking was observed to be nearly twice as effective as clocking stators, while clocking successive blade rows, (*i.e.* two stator rows and the rotor rows between) produced a change in efficiency 2.45 times that of single stator clocking alone. Similar to the stator clocking rotor efficiency was optimal when the upstream rotor wake impinged on the leading edge of the clocked rotor airfoil.

Three-dimensional effects of clocking were studied by Dorney and Sondak [27] based on the UTRC LSRR geometry. Contrary to compressor studies [22, 23] mid-passage efficiency was shown to be relatively constant. Higher amplitudes of unsteadiness were observed at minimal efficiency, however, this was predominantly at the blade passing frequency, whereas high frequency unsteadiness corresponded to higher efficiency. The greatest efficiency changes were observed from 0-20% span and 95-100% span, corresponding to the largest changes in pressure and exit flow angle denoting higher work between these spanwise ranges. Blade loading was observed as almost constant across the span.

Huber *et. al.* [28] performed perhaps the most extensive experimental clocking study on the Space Shuttle Main Engine Alternative Turbopump Design. Herein both thermal and mechanical design efficiencies were investigated against first-stage stator circumferential position, Reynolds number (by decreasing inlet pressure), and wheel speed (Ω). At the design point both optimal and minimal clocking positions were defined. Then by varying the wheel speed from 2000 - 10,000 rpm, and the inlet Reynold's number, the operational limit of these two points were further defined. Efficiency (both thermodynamic and mechanical) was observed to increase asymp-

totically with speed parameter, illustrating a small bias, that was undetermined. Efficiency, based on clocking position, followed the same pattern as previous clocking studies, resulting in a periodic trend. Reduced Reynolds number proved to decrease measured efficiency.

As a companion to Huber *et. al.* [28], Griffin *et. al.* [29] performed a computational study to further investigate the measured effects of Huber *et. al.*, at the engine design point. The study consisted of a two-dimensional computational fluid dynamic investigation using modified blade counts to reduce computational strain. Total-to-total efficiency was used to determine effectiveness of each clocking position. Average η_{tt} in the computational model was observed to be 87.90% with an average $\Delta\eta_{tt}$ of $\pm 0.40\%$ while the experimental study showed an average efficiency of 94.80% with an average $\Delta\eta_{tt}$ of $\pm 0.15\%$. Discrepancies in the two results was attributed to two main factors: a) low aspect ratio of the turbine which causes some spanwise mixing, and b) three-dimensional effects that are not captured in a two-dimensional study. However, local maximum and minimum clocking positions were in agreement with the experimental study.

1.3 Previous Results

The extensive hot streak research using the United Technologies Research Center's Large Scale Rotating Rig and NASA's Combustor Exit Radial Temperature Simulator has demonstrated the following conclusions:

1. Hot streaks and cold streaks segregate from the free stream flow due to:
 - (a) Incidence and velocity differences from the free stream
 - (b) Secondary flows from the endwalls

2. If the hot streak is three-dimensional in nature a three-dimensional analysis is required, whereas two-dimensional codes are adequate for planar hot streaks
3. Secondary flows in the rotor passage cause migration of hot streaks to the endwalls of the airfoils
4. Hot streaks migrate to the pressure surface whereas cold streaks migrate to the passage
5. Clocking of the hot streak to impact the first-stage stator reduces the surface heating effects of hot streaks on aft blade rows
6. The greatest surface heating due to hot streaks is found at the airfoil endwalls (hub and tip) producing local hot spots and thus local blade burning
7. Elliptical hot streaks dissipate more readily than circular hot streaks due to higher surface area in contact with the cooler free stream flow
8. Rotor surface temperatures are strongly dependant on hot streak radial and circumferential introduction

Clocking studies present less definite findings. Results prove to be geometry and boundary condition driven, however, some general trends are observed:

1. Rotor losses are inversely related to stator losses, corresponding to efficiency peaks, and troughs
2. Efficiency is directly related to the positioning of the clocked row, as proper alignment affects the upstream rotor potential field resulting in greater flow turning and higher efficiency

3. The highest efficiency occurs when upstream wakes are made to impinge the clocked airfoil leading edge
4. Simulations of equal blade counts downplay potential flow in the simulation, resulting in greater observed efficiencies
5. Maximum and minimum efficiencies vary by approximately one half stator pitch

1.4 Current Investigation

The current study is to contain a hot streak simulation based on the UTRC LSRR geometry, as well as a multi-stage clocking study based on a proprietary turbine geometry. These two simulations will provide insight into the effects of unsteadiness management in turbomachines. Proving that, if properly designed, turbine blading can provide increases in efficiency (typically 0.5% through clocking) and experience elevated life spans and increased durability by decreasing the thermal loading (*i.e.* hot streak management) and through clocking by utilizing the entropy wasted in poorly aligned airfoils.

The hot streak study is based on a temporally oscillating hot gas intrusion at various frequencies from constant (0.00 BPF), to unity (1.00 BPF) as normalized by the blade passing frequency. The simulation will be two-dimensional, taken at mid-span. The imposed hot streak models a planar hot streak. Thermal quantities such as loading and propagation are of interest in addition to frequency dependency, with particular interest to the rotor blading.

The clocking study results are presented based on the clocking of a third-stage nozzle with respect to the second-stage nozzle. Simulations are run at eight clocking positions, from baseline to maximum based on one stator pitch. Stage efficiency, as

related to clocking position, as well as machine efficiency will be discussed as normalized quantities as a function of the clocked blade row quantities. Losses for both rotating and non-rotating rows will also be investigated.

CHAPTER 2 Numerical Integration Procedure

The computational code used in the current study is known as WILDCAT and is a NASA code developed and maintained by Dr. Daniel J. Dorney. It is a derivative of the CORSAIR family of codes and is a fully implicit, time marching, upwind, finite difference Navier-Stokes code solving on structured grids. It is third-order spatially accurate and second-order temporally accurate. The code has been parallelized using message passing interface (MPI and OpenMP) libraries allowing simulations to be decomposed arbitrarily depending on the number of available processors. The governing equations in the current study are time-marching, two-dimensional Navier-Stokes equations, represented below in cartesian coordinates.

$$U + (F_i + F_v)_x + (G_i + G_v)_y = 0 \quad (2.1)$$

where U represents the conserved flow variables in the form:

$$U = \begin{bmatrix} \rho \\ \rho u \\ \rho v \\ e_t \end{bmatrix} \quad (2.2)$$

and F and G represent the components of viscous and inviscid mass, momentum, and energy fluxes:

$$F_i = \begin{bmatrix} \rho u \\ \rho u^2 + P \\ \rho uv \\ (e_t + P)u \end{bmatrix} \quad F_v = - \begin{bmatrix} 0 \\ \tau_{xx} \\ \tau_{xy} \\ \tau_{hx} \end{bmatrix} \quad (2.3)$$

$$G_i = \begin{bmatrix} \rho v \\ \rho v^2 + P \\ \rho uv \\ (e_t + P)v \end{bmatrix} \quad G_v = - \begin{bmatrix} 0 \\ \tau_{yx} \\ \tau_{yy} \\ \tau_{hy} \end{bmatrix} \quad (2.4)$$

where the energy, viscous, and inviscid flux terms are defined as:

$$\begin{aligned} \tau_{xx} &= 2\mu u_x + \lambda(u_x + v_y) \\ \tau_{xy} &= \mu(u_y + v_x) \\ \tau_{yx} &= \tau_{xy} \\ \tau_{hx} &= \mu\tau_{xx} + v\tau_{xy} + \gamma\mu P_r^{-1}e_x \\ \tau_{hy} &= \mu\tau_{yx} + v\tau_{yy} + \gamma\mu P_r^{-1}e_y \\ e &= \frac{P}{(\rho(\gamma-1))} \\ e_t &= \rho e + \frac{\rho(u^2+v^2)}{2} \end{aligned} \quad (2.5)$$

The second coefficient of viscosity is calculated using Stokes' hypothesis, $\lambda = -2/3\mu$. The perfect gas law is then applied to complete the equations of motion. To extend the equations of motion to turbulent flows, an eddy viscosity formulation is employed.

Thus, the effective viscosity and effective thermal conductivity can be defined as:

$$\begin{aligned}\mu &= \mu_L + \mu_T \\ \frac{\kappa}{C_p} &= \frac{\mu_L}{P_{r,L}} + \frac{\mu_T}{P_{r,T}}\end{aligned}\tag{2.6}$$

The turbulent viscosity is calculated through a highly modified form of the Baldwin-Lomax [30] turbulence model.

The numerical procedure used for the two-dimensional analysis discretizes inviscid fluxes according to the scheme developed by Roe. In addition, Newton subiterations are used at each global time step to increase the stability and reduce the linearization errors.

CHAPTER 3 Geometry

The test geometry for the hot streak study is that of the United Technologies Research Center (UTRC) Large Scale Rotating Rig (LSRR). The LSRR is an open circuit type $1\frac{1}{2}$ stage large scale rotating rig with 22 first-stage stator airfoils, 28 first-stage rotor airfoils, and 28 second-stage stator airfoils. The mid-span radius is 27 inches with a 6 inch span of constant cross-section (untwisted). An accurate approximation of this geometry would be 11-14-14. However, the current simulation is based on a 1-1-1 blade count, which is achieved by increasing the number of stators in the first-stage stator row to 28 and then scaling the airfoils to retain the actual blockage via blade counts (corrected using the factor of $(\frac{\text{number of initial blades}}{\text{number of scaled blades}})$). Then by assuming circumferential periodicity of flow fields the final gridding can be reduced to a 1-1-1 simulation.

A large amount of experimental data exists for this geometry including pressure data before, aft, and along each of the airfoils. Also, there are a considerable number of previous studies conducted for this geometry allowing for accurate conclusions to be drawn from the current study.

The clocking study test geometry consists of 4 stages of a Solar Turbines, Inc. industrial turbine. The blade count in the actual turbine is 48-88-68-82-68-64-39-58. Inspection of this blade count reveals that the second and third-stage nozzle vanes are candidates for airfoil clocking. In the simulations a 50-90-70-80-70-60-40-60 blade count was modeled. The airfoil geometries were scaled in the same manner as the

airfoils in the hot streak case. This resulted in a reduced number of passages in the simulation, since it can be modeled with a 5-9-7-8-7-6-4-6 blade count with periodic boundary conditions applied in the circumferential direction.

It is important to note that the simplification of these actual blade counts provides a reasonable compromise between accuracy of the model and feasible computation times for both cases. This has an additional effect in the clocking, producing clocking effects in the third and fourth-stage rotors which do not occur in the actual turbine.

CHAPTER 4 Gridding

An O-H zonal grid system was used to discretize the flow field within both turbine test geometries. The H-grids are algebraically generated and are used in regions upstream of the leading edge, downstream of the trailing edge, and in the interblade region and are allowed to move relative to each other simulating blade rotation. O-grids are body fitted to the airfoils using an elliptical equation solver to properly resolve the viscous flow characteristics in the blade passages and to apply easily the algebraic turbulence model. Computational grid lines in the O-grids are stretched in the blade-normal direction with fine grid spacing at the wall. For the current two-dimensional simulations the O-grids are overlaid onto the H-grids. O-grid dimensions are determined by the values of y^+ , the normalized distance of the first point above the airfoil, the number of points within the boundary layer and computational time required to complete the simulations. H-grid densities were determined by performing wake convection simulations in the absence of the airfoils. Further explanation of the O-H zonal meshing can be found in Refs. [15, 32].

There are two computational grids used for the hot streak study, one coarse and one fine. The O-grids for the three blade rows in the coarse grid each contained 251×41 (streamwise X tangential) grid points. The H-grids for the first-stage stator passage contained 145×45 grid points, the H-grid for the rotor passage contained 109×45 grid points and the H-grid for the second-stage stator contained 110×45 grid points. Thus, the complete grid system for the turbine contained 46,253 grid points. The

O-grids in the fine grid case were unchanged from that of the coarse grid, but the H-grids were incrementally refined until they could accurately propagate the flow. The resulting H-grids for the fine grid study are 201×45 for the first-stage stator, 251×45 for the first-stage rotor and 250×45 for the second-stage stator.

The O-grids for all blade rows in the clocking study contained 121×35 (streamwise X tangential) grid points. The H-grids for each blade row averaged 125×35 grid points. Thus the complete grid for the test turbine contained 425,552 grid points. The average y^+ was approximately 1.0 for all blade rows. The boundary layers were discretized with 10-15 grid points. Figures 4.1 and 4.2 show the computational gridding for the full computational domain and a close up of the Nozzle 2 - Nozzle 3 region, where the clocking will be applied.

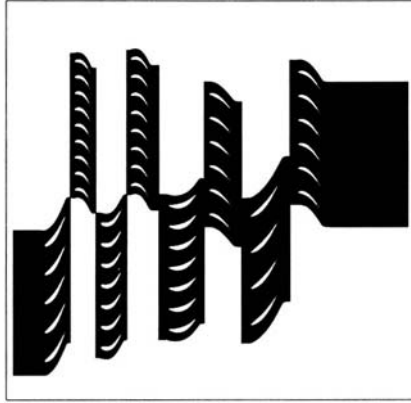


Figure 4.1: Full Computational Grid - Clocking Case.

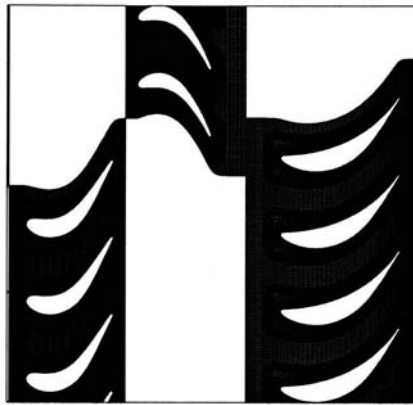


Figure 4.2: Close Up of Nozzle 2 - Nozzle 3 Computational Grid - Clocking Case.

CHAPTER 5 Boundary Conditions

For subsonic inlet flow, the total temperature, total pressure, flow angle, and Mach Number, are imposed while the upstream running Riemann invariant, $R_1 = u - \frac{2a}{\gamma-1}$, is extrapolated from the interior of the computational domain. Inlet flow boundary conditions within the hot streak are updated using Riemann invariants where the velocity and speed of sound reflect the static and stagnation temperature increase in the hot streak. The static and total pressures in the hot streak are assumed equal to that of the undisturbed inlet flow. For subsonic outflow, the pressure ratio P_{exit}/P_{t0} is specified while the v velocity component, entropy, and the downstream running Riemann invariant, $R_2 = u + \frac{2a}{\gamma-1}$ are extrapolated from the interior of the computational domain. No-slip boundary conditions are enforced at all solid walls. Periodicity is enforced along the outer boundaries of the H-grids in the circumferential direction. In the present study, the walls are assumed to be adiabatic.

In the hot streak study computations were performed using a flow coefficient of 0.78, a pressure ratio of 0.9505 calculated from P_3/P_{t0} , and a rotor rotational speed (Ω) of 410 rpm. Inlet flow was assumed axial and the inlet absolute Mach number was 0.7. The average value of y^+ , the nondimensional distance of the first grid point above the surface, was approximately 0.5 for all three blade rows. The boundary layers (on average) were discretized with 15-20 grid points. The simulations were performed on three 275 MHz R12000 processors of an SGI Origin 200 workstation. Each simulation ran for a total of 125 rotor blade passing cycles to ensure time-

periodicity over a broad range of frequencies, requiring approximately 40 hours of computation time per run. Each case was time-averaged over 10 hot streak cycles except for the constant case, where it was time-averaged over 10 rotor blade passing cycles.

Inlet imposition of the hot streak introduces two fundamental assumptions: a) the pressure within the hot streak, both static and total (P_s and P_t) are equal to that of the undisturbed inlet flow, and b) the Mach number within the hot streak is also equal to that of the free stream inlet flow [3]. Based on these assumptions and applying the perfect gas equation (Eqn. 5.1) to the Mach number equation (Eqn. 5.2) the following relations are obtained (see Eqn. 5.3).

$$P = \rho \cdot R \cdot T \quad (5.1)$$

$$M = \frac{V}{\sqrt{\gamma \cdot R \cdot T}} \quad (5.2)$$

$$\begin{aligned} a_{HS} &= a_{\infty} \sqrt{\frac{T_{HS}}{T_{\infty}}} \\ u_{HS} &= u_{\infty} \sqrt{\frac{T_{HS}}{T_{\infty}}} \\ v_{HS} &= v_{\infty} \sqrt{\frac{T_{HS}}{T_{\infty}}} \\ P_{HS} &= P_{\infty} \\ \rho_{HS} &= \rho_{\infty} \cdot \frac{T_{\infty}}{T_{HS}} \end{aligned} \quad (5.3)$$

For clocking simulations the inlet flow to the first-stage stator was axial with an inlet Mach number of 0.136, a total pressure of $P_{t_1} = 1.60 MPa$ and a total temperature of $T_{t_1} = 1420^\circ K$. The inlet Reynolds number was approximately 2×10^6 based on the first-stage stator axial chord. The first two stages of this geometry rotate at 10,942 rpm, whereas the last two stages rotate at 9,187 rpm. In keeping with the

geometry of the flowpath, the streamtube ratios varied from 1.0 to at the inlet to the first-stage nozzle to 4.05 at the exit of the fourth-stage rotor. An arbitrary clocking position was chosen in order to calculate the baseline flow field. For this study it is important to note that non-reflecting boundary conditions were not used due to slight mass flow variations that can occur when blockage changes due to clocking. A total of eight (8) simulations were performed in which the third-stage nozzle was clocked with respect to the second-stage nozzle. All computations were performed using one Newton subiteration per time step and 54,000 time steps per global cycle. In the context of this study a global cycle is defined as the time it takes the nine (9) first-stage rotors to pass by the five (5) first-stage stators. A baseline calculation was run for ten (10) cycles (one complete rotor revolution). Each clocking simulation, which was initiated by the baseline solution was run for an additional rotor cycle to ensure time-periodicity and the inclusion of all relevant frequencies. Time-averaged quantities were averaged over five (5) global cycles. Computations were performed on eight processors of an SGI Origin 2000 workstation with 250 MHz R12000 processors. Each simulation approximately 2×10^{-6} seconds/grid point/iteration computational time.

CHAPTER 6 Hot Streak Results

The general form of the time-dependent hot streak temperature variations is given by:

$$T_{HS} = T_{Base} + T_{amp} \sin(2\pi * N * fm + \phi) \quad (6.1)$$

where T_{Base} is the nominal hot streak temperature, N is the rotor blade passing frequency and fm is the frequency of the hot streak unsteadiness normalized by the blade passing frequency and ϕ allows for phase variations. Simulations were conducted at 0.00, 0.25, 0.50, 0.75, and 1.00 times the blade passing frequency. Note, 0.00 BPF refers to a hot streak of constant temperature, and is characteristic of previous studies [7, 17, 31]. The frequencies chosen for this study are the result of communication with combustor experts [33]. In addition, to the previously mentioned simulations, three supplemental studies were performed; one at 1.0 BPF in which the phase was modified by half the rotor blade passing frequency, one at 0.50 BPF with the second stage stator clocked by one half the stator pitch, and one at 1.00 BPF with the hot streak synchronized with the rotor blade passing frequency and the second stage-stator clocked to one half the stator pitch. The nominal hot streak temperature profile models that of a planar hot streak introduced mid-pitch between two adjacent first-stage stator airfoils and covers one-quarter of the blade pitch. The current study involves a grid resolution study determining an adequate mesh to facilitate proper convection of the hot gas in time as hot streak frequency increases.

Frequency effects are separated into two sub-groups a) frequencies below unity (1.00 BPF) and hot streak frequency at unity. A clocking study was also employed at two hot streak frequencies (0.50 and 1.00 BPF) to determine the effectiveness of clocking the second stator with respect to the hot gas.

CHAPTER 7 Hot Streak Grid Resolution Results

Grid definition becomes increasingly more important when additional time dependence is added to the flow. Given this, the gridding requirements for this study are considerably more stringent than those of previous studies. The ‘coarse’ grid described previously is representative of grid densities used in previous studies, whereas the ‘fine’ grid was determined through incrementally increasing the H-grid density in the axial direction.

Time-averaged temperature contours for both 0.00 and 0.50 BPF are shown below (Fig. 7.1 and Fig. 7.2). Qualitatively, both cases appear to be the same, except that the fine grid allows for more accurate convection throughout the passage. The most noticeable of this is shown in the rotor vortex sheet, which is more clearly defined by the fine grid. This is expected since there is a smaller inter-grid point gap to allow for computational error. As frequency increases the coarse grid is unable to handle the increased need by time variance of temperature intrusion. This deficiency is alleviated by using the fine grid.

Inlet and exit profiles of each blade passage offer a much greater qualitative grasp of the need for the fine grid system. In both the 0.00 and 0.50 BPF (see Figs. 7.3 and 7.4) cases, the stator-one inlet profiles for the coarse grid have sharp transitions. However, using the fine grid, the sharp transitions are almost completely eliminated

from the profile while the general shape remains the same across the passage. This is also the case in the stator-one exit profiles, however, the fine grid denotes that the general profile is translated to the left and that the overall temperature reaches approximately 1.15 in both cases. This is considerably higher than the 0.50 case, showing an almost 30% increase in maximum temperature, and the same for the 0.00 case only to a lesser degree with an approximate 2% increase in maximum temperature.

Rotor exit profiles also depict lateral translation as well as temperature attenuation by the coarse gridding. However, in the rotor passage, the hot streak at 0.00 BPF is more attenuated by the gridding, whereas the 0.50 BPF case is more drastically distorted spatially. In addition, fine grid temperature profiles for this passage do not exhibit the same general shape as the coarse grid profiles (see Figs. 7.5 and 7.6). More important than the rotor exit profile is the rotor surface profile. Due to cooling regimes for rotating rows being more difficult to manufacture it is imperative that the true blade loading be represented. In agreement with preceding data, Figs. 7.7 and 7.8 indicate that higher grid definition results in an increase in measured temperatures on the surfaces of the airfoil.

The trends exhibited in the temperature profiles are consistent with those expected for a hot streak entering between two adjacent first-stage stators. Additionally, it is noted that as frequency increases so does the rotor surface temperature. Grid refinement was observed to produce qualitatively similar results that vary in magnitude and placement throughout the stage.

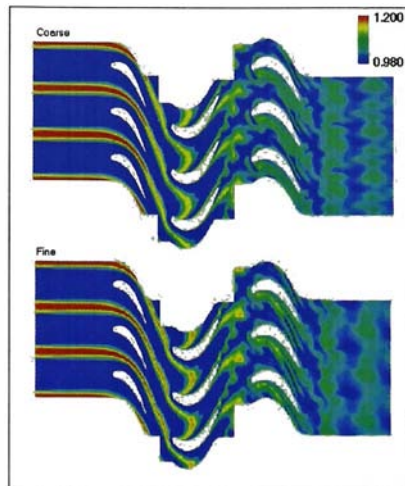


Figure 7.1: Instantaneous Static Temperature Contours - 0.0 BPF.

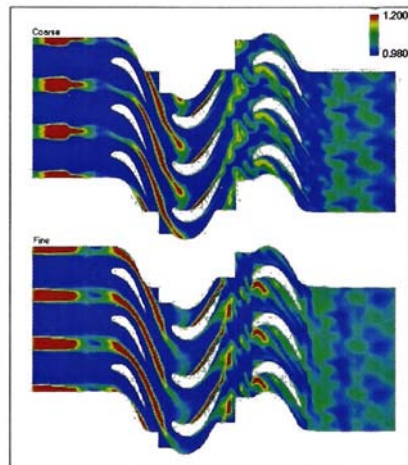


Figure 7.2: Instantaneous Static Temperature Contours - 0.5 BPF.

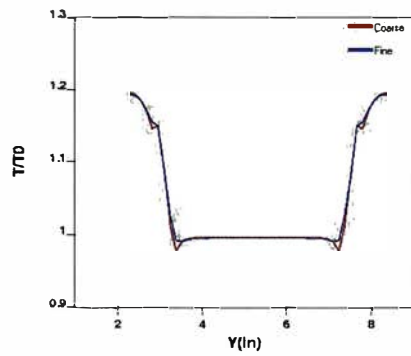


Figure 7.3: Time-Averaged Total Temperature - 0.00 BPF - Stator 1 Inlet.

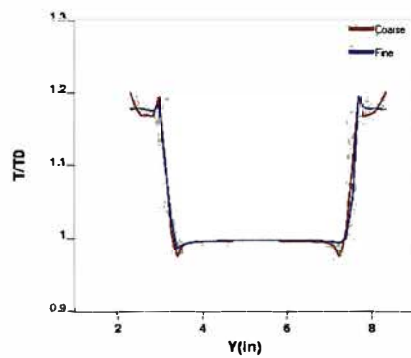


Figure 7.4: Time-Averaged Total Temperature - 0.50 BPF - Stator 1 Inlet.

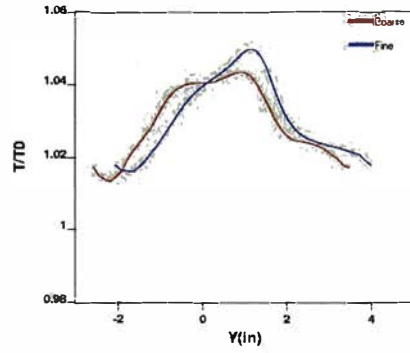


Figure 7.5: Time-Averaged Total Temperature - 0.00 BPF - Rotor 1 Exit.

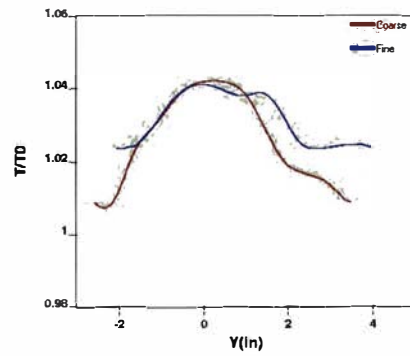


Figure 7.6: Time-Averaged Total Temperature - 0.50 BPF - Rotor 1 Exit.

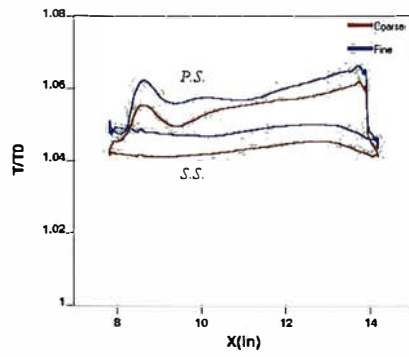


Figure 7.7: Time-Averaged Total Temperature Surface Profile - 0.00 BPF - Rotor 1 .

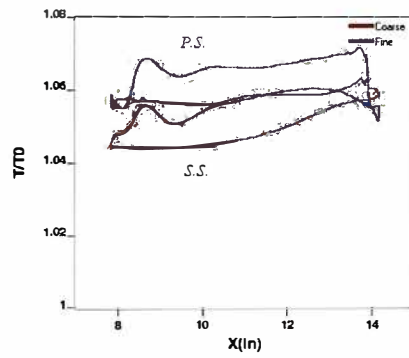


Figure 7.8: Time-Averaged Total Temperature Surface Profile - 0.50 BPF - Rotor 1.

CHAPTER 8 Hot Streak Results at Frequencies Less Than Unity

Hot streak frequencies less than rotor blade passing frequency are most representative of those found in modern axial turbines [33]. Knowledge of the effect that these lower frequencies have on airfoil surface temperatures should prove useful to combustor designers such that fuel nozzles can be modified to dissipate these low frequency oscillations in temperature.

Figure 8.1 shows the exit profiles for the first-stator at varying hot streak frequencies. The first-stage stator exit profile shows a gradual decrease in temperature as the hot streak frequency approaches unity. This is due to hot streak periodicity effects.

Figure 8.2 shows the progression of temperature with respect to hot streak frequency. As shown, at frequencies below 0.75 BPF, the surface temperature profile exhibits an increasing trend. The surface thermal profiles are consistent with previous hot streak experiments [13, 34], such that the pressure surface exhibits higher temperatures with a nearly linear slope from the point of impaction, than the suction surface. This is can most likely be attributed to the physical characteristics of hot streak propagation based on the Kerrebrock-Mikolajczak Effect, with blade shape accounting for the decrease, then increase in temperature just after the point of impact. Even with this characteristic increase in temperature, at most pressure surface heating shows a 0.8% temperature increase relative to the suction surface for frequencies above 0.00 BPF. This is approximately one third of that experienced at 0.00 BPF (2.4%). Overall hot streak frequency does not exhibit a strong contribution to rotor surface heating

for frequencies in this range. This is made evident by the relatively low change in temperatures between the cases (*i.e.* maximum suction and pressure surface temperature variations are less than 2% based on hot streak frequency).

Figure 8.3 shows the rotor passage exit profiles. As can be seen the constant case produces the greatest time-averaged temperature profile at the stage exit, though all cases produce qualitatively similar results. Contrary to the rotor surface profile the stage exit shows a consistently declining maximum temperature. This can be attributed to the increased dissipation of the hotter fluid via shorter localized temperature maximums within the passage.

The second-stage stator surface temperature profile is seen in Fig. 8.4. Initial viewing of these results show a similar trend to that of the first-stage rotor surface profile. Both the 0.00 and 0.25 BPF cases and the 0.50 and 0.75 BPF cases show similarities, though the greater heating within each group is at the higher frequency (*i.e.* between the 0.00 and 0.25 BPF, the 0.25 BPF exhibits the greater temperatures on the airfoil). This is due to the amount of hot fluid passing through the rotor passage and impacting on the airfoil surface. As shown by the passage exit profile (Fig. 8.3), both the 0.25 and 0.75 BPF cases show a local maximum near $Y \approx 2.00$ whereas the 0.00 and 0.50 BPF cases do not have as pronounced a maximum at this location, however, both the 0.00 and 0.75 BPF possess a prominent localized maximum at $Y \approx 3.75$ thereby accounting for the increased surface temperatures at 0.25 and 0.75 BPF and the increased passage temperatures at 0.00 and 0.75 BPF.

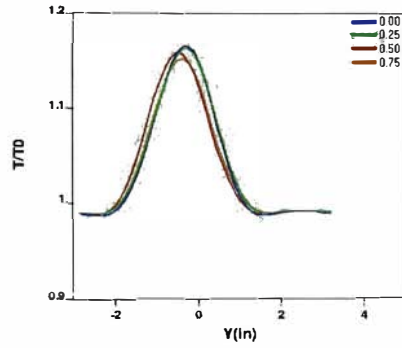


Figure 8.1: Time-Averaged Total Temperature - Stator 1 Exit.

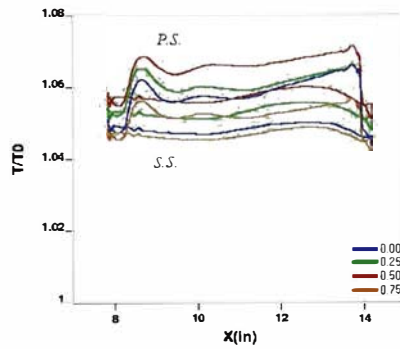


Figure 8.2: Time-Averaged Total Temperature Surface Profile - Rotor 1.

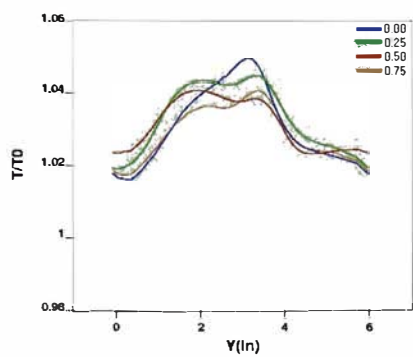


Figure 8.3: Time-Averaged Total Temperature - Rotor 1 Exit.

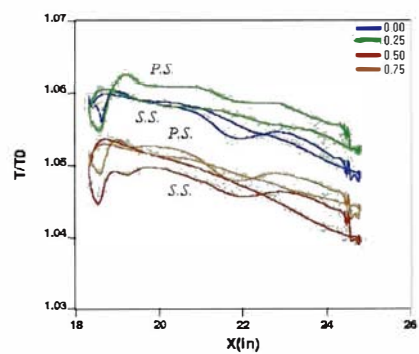


Figure 8.4: Time-Averaged Total Temperature Surface Profile - Stator 2.

CHAPTER 9 Hot Streak Results at Unity

At hot streak frequencies of unity a unique phenomenon takes place that is particularly beneficial to designers. Shown in Figs. 9.1 and 9.2 illustrate the stator 1 inlet and exit profiles respectively, where nominal is synonymous with baseline, whereas the 180° offset was achieved by running the case without the hot streak intrusion for half of one rotor cycle and then ‘turning on’ the hot streak for the remainder of the simulations. Cursory viewing of Figs. 9.1 and 9.2 in conjunction with the exit profiles for frequencies less than unity suggests considerable agreement with each other.

However, at 1.00 BPF, the rotor surface heating is significantly lower than any of the cases below unity for the nominalized case (see Fig. 9.3). Comparatively, with a 180° phase shift imposed on the hot streak the rotor shows more surface heating than in any other case. This gives rise to the conclusion that if hot streaks are made to pulsate in phase with the rotor blade passing frequency, it can be made such that the hot streak misses the rotor blading entirely, passing completely through inter-rotor passage. Figure 9.4 shows the stage exit profile. Here the nominal case shows a nearly perfect sine wave spatial periodicity as would be expected from an uninhibited propagation through the passage, whereas the phase shifted case shows a sinusoid with an additional frequency, such as that of the rotor interaction with the hot streak.

This propagates directly to the second-stage stator surface temperature profiles (Fig. 9.5). In the nominal case, stator 2 is experiences greater thermal loading than

during the phase shifted case. This is due to the amount of hot fluid passing directly through the rotor passage without impacting the rotor. Though this increases the loading of the second stage stator, it reduces the loading on the rotor, allowing for ease of application of cooling flows since it is easier to cool non-rotating rows than rotating rows due to the inherent unsteadiness associated with rotating airfoils.

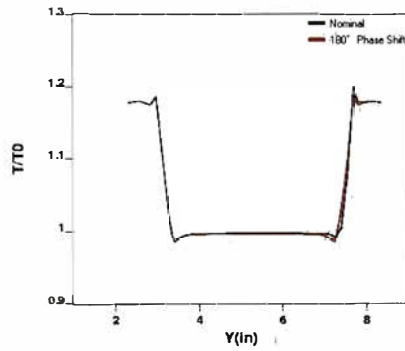


Figure 9.1: Time-Averaged Total Temperature - Stator 1 Inlet - 1.00 BPF.

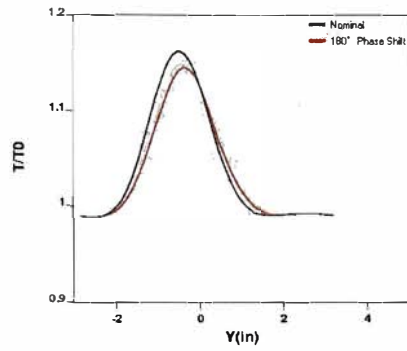


Figure 9.2: Time-Averaged Total Temperature - Stator 1 Exit - 1.00 BPF.

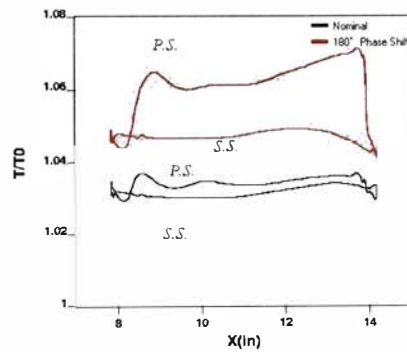


Figure 9.3: Time-Averaged Total Temperature Surface Profile - Rotor 1 - 1.00 BPF.

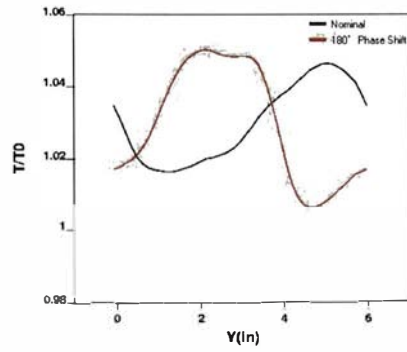


Figure 9.4: Time-Averaged Total Temperature - Rotor 1 Exit - 1.00 BPF.

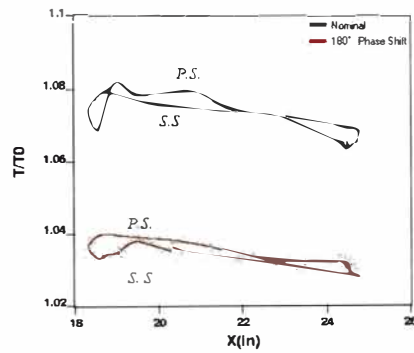


Figure 9.5: Time-Averaged Total Temperature Surface Profile - Stator 2 - 1.00 BPF.

CHAPTER 10 Clocking Effects on Hot Streak Migration

Traditionally, hot streaks are ‘clocked’ by forcing them to impinge on the leading edge of the first-stage stator, in this case, given the flow characteristics of hot streaks oscillating at the rotor blade passing frequency, the second-stage stator has been clocked to half pitch, or offset by half the passage Θ , where Θ is:

$$\Theta = \frac{2 \cdot \pi}{\text{number of blades}} \quad (10.1)$$

After applying this clocking to the initial solution and re-running the simulation based on the nominalized position the temperature field for the full $1\frac{1}{2}$ stages is seen in Fig. 10.1. Notice, how clocking forces the hot streak to miss not only the rotor but the stator as well. Rotor 1 and stator 2 surface profiles are seen in Figs. 10.2 and 10.3 respectively. In both cases the thermal loading is reduced to values significantly lower than previously observed lows (nominal for rotor 1 and phase shifted for stator 2). However, due to the flow being forced to travel through almost entirely through the passages, the suction surfaces of both airfoils exhibit the greatest thermal loading. This effect can be alleviated or exaggerated by changing the relative position of the blade rows with respect to the hot streak.

In comparison to the clocked and synchronized case (Fig. 10.1) an additional simulation was performed at 0.50 BPF. Time-averaged temperature is shown in Fig. 10.4.

Clocking the second-stage stator produced trends identical to the 1.00 BPF for both the stage and on the surface profile of stator 2 (Fig. 10.5), decreasing the maximum total temperature by approximately 4% on the airfoil and producing greater temperatures on the suction surface than on the pressure surface.

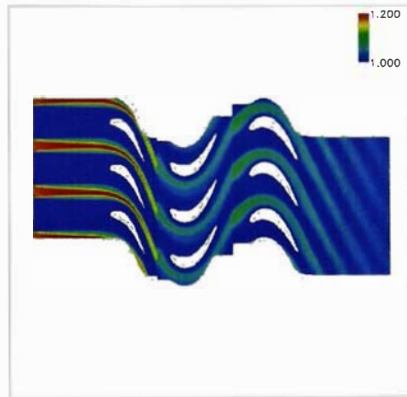


Figure 10.1: Time-Averaged Total Temperature - 1.00 BPF - Clocked and Synchronized.

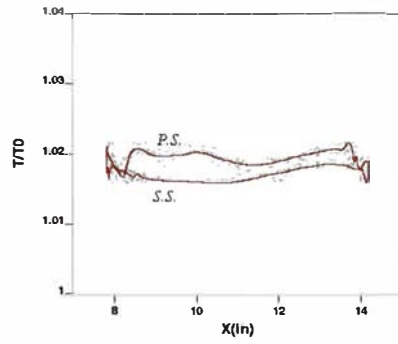


Figure 10.2: Time-Averaged Total Temperature Surface Profile - Rotor 1 - 1.00 BPF - Clocked and Synchronized.

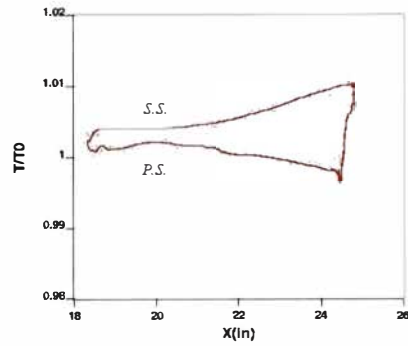


Figure 10.3: Time-Averaged Total Temperature Surface Profile - Stator 2 - 1.00 BPF - Clocked and Synchronized.

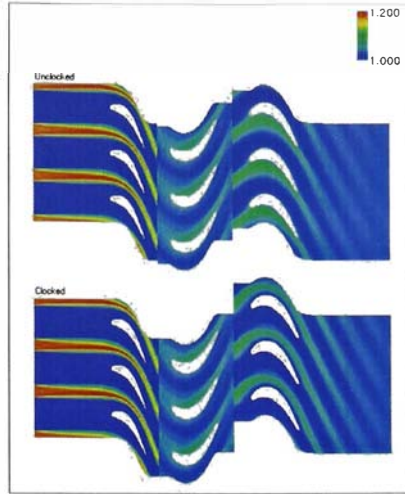


Figure 10.4: Time-Averaged Total Temperature - Stator 2 Clocked - 0.50 BPF.

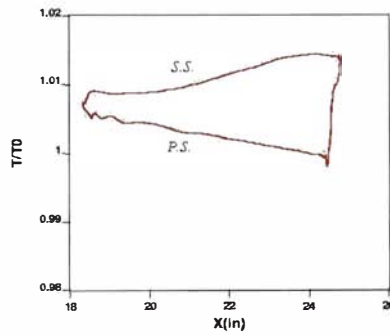


Figure 10.5: Time-Averaged Total Temperature Surface Profile - Stator 2 Clocked - 0.50 BPF.

CHAPTER 11 Embedded Stage Clocking Results

Mach contours for the entire turbine are shown in 11.1, and a close-up of vane 2 - vane 3 instantaneous Mach number is shown in 11.2. Vortex shedding is evident from the vane 2 airfoils. Convection of the vane 2 wake through the rotor passage exhibits a 'V' profile entering the vane 3 passage. This is a product of differing velocities on the rotor pressure and suction surfaces. In addition, as the wake convects through the passage it is turned more axial. The placement of this wake in the vane 3 passage is directly responsible for clocking effects.

Instantaneous (non-dimensional) entropy contours are shown at high efficiency for the full turbine Fig. 11.3 and for the vane 2 - vane 3 region Fig. 11.4. Increasingly complex wake patterns are shown in the full turbine, as is characteristic with the addition of blade rows. The close-up of vane 2 - vane 3 again illustrates the vortex shedding within the second stage vane wake. Time-averaged entropic flow fields again highlight the wake passing from the second-stage vane to the third for both high and low efficiencies in Figs. 11.5 and 11.6, allowing a better representation of the stage 2 wake to vane 3. When vanes are clocked to a position yielding high efficiency, the upstream wake is shown to impinge on the leading edge of the clocked airfoil, conversely, when the wake is made to pass mid-passage the low efficiency position is observed.

Efficiency variation for the four stages of the turbine is shown as a function of third stage clocking position in Fig. 11.7. In this study the total-to-total efficiency is

defined per stage as (using stage one for reference):

$$\eta_{tt} = \frac{1.0 - T_{t2}/T_{t0}}{1.0 - (P_{t2}/P_{t0})^{(\gamma-1)/\gamma}} \quad (11.1)$$

The angular offset, θ_{off} refers to the circumferential displacement of the third-stage vane leading edge relative to the trailing edge of the second-stage vane. Positive displacement coincides with rotor rotation direction. As should be expected the variation in efficiency in the first two stages is minimal as the third-stage is clocked. The third stage exhibits significant changes in efficiency ($\pm 0.25\%$) with clocking position, while the fourth stage shows modest variations ($\pm 0.15\%$). This is due to the third-stage wake entering the fourth-stage at differing circumferential positions. As seen, efficiency for the third and fourth stages appear to be nearly 180° out of phase with the third stage, this stems from the relative position of the third-stage rotor to the fourth-stage rotor at the baseline conditions, thus when the third-stage is clocked to the maximum efficiency position, the third-stage rotor wake lies nearly mid-passage in the fourth stage-rotor. Variation in total turbine efficiency corresponds to efficiency positions for the third-stage, showing lower overall variations ($\pm 0.05\%$). However, this value should increase, due to clocking effects in the computational model that do not exist in the actual machine.

Scaled loss variations for the stator and rotor rows are seen in Figs. 11.8 and 11.9 respectively. Neither of the first-stage airfoils showed significant variations with clocking position, the second-stage shows minimal discrepancies due to potential effects from clocking. Vane losses in the third stage follow the same trend as the efficiency (*i.e.* higher losses correspond to higher efficiencies), where rotor losses have an inverse trend with efficiency. It is important to note that the actual decrease in rotor loss was greater than the increase in vane loss. The fourth stage trends are opposite those of the third.

Unsteady pressure envelopes (shown at maximum efficiency) are shown in Figs. 11.10 to 11.13. The first stage shows minimal unsteadiness, and that which is present downstream of the throat can be attributed rotor potential field interaction. Vanes in the second (Fig. 11.11), third (Fig. 11.12), and fourth stages (Fig. 11.13) show modest unsteadiness resulting from wake interactions from upstream blade rows and potential effects from adjacent blade rows. Comparisons between maximum and minimum efficiency blade loading for vanes 2 and 3 is shown Figs. 11.14 and 11.15. Vane 2 shows almost no variation with clocking where vane 3 shows considerably more unsteadiness at the higher efficiency than at the lower, corresponding loss variation for vane 3. Maximum and minimum unsteady pressure histories taken at the vane 3 leading edge are illustrated in Fig. 11.16. The traces are nearly 180° out of phase which is consistent with entropy contours in Figs. 11.5 and 11.6, and vane 3 losses (Fig. 11.12).

Unsteady pressure envelopes for the rotor blading are shown in Figs. 11.17 to 11.20. Consistent with entropy contours, the rotor shows increasing unsteadiness with axial progression due to increased wake/airfoil interaction and potential flow effects. Maximum and minimum pressure envelopes for rotor 2 and rotor 3 are illustrated in Figs. 11.21 and 11.22 respectively. Similar to the vane 2 results the rotor 2 pressure envelope is nearly unaffected by vane 3 clocking position. In contrast to the vane 3 results, the amplitude of the rotor 3 unsteadiness is greater at the clocking position corresponding to high efficiency.

Time-averaged absolute exit flow angle, as a function of third-stage clocking position, for the vane rows are shown in Figs. 11.23 to 11.26 respectively. Neither of the first 2 stages show significant variation with respect to clocking position (maximum variation of approximately $.005^\circ$). Vane 3 is the only vane that shows significant variation with clocking position, varying approximately in phase with efficiency. This

variation in turn propagates to the third stage rotor, thus altering the stage work and efficiency.

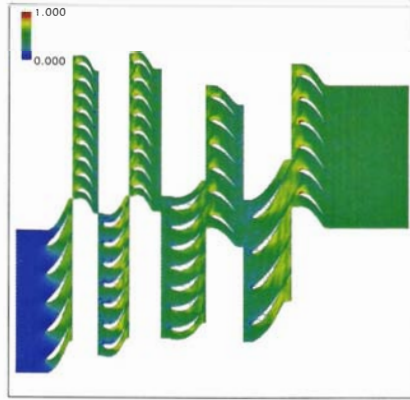


Figure 11.1: Full Annulus Instantaneous Mach Contours - High Efficiency.

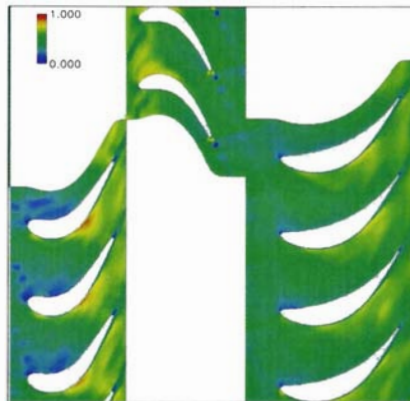


Figure 11.2: Nozzle 2 - Nozzle 3 Instantaneous Mach Contours - High Efficiency.

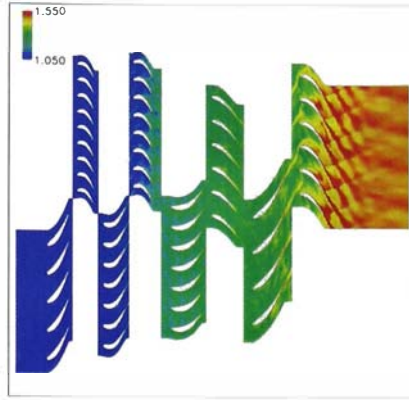


Figure 11.3: Full Annulus Instantaneous Entropy Contours - High Efficiency.

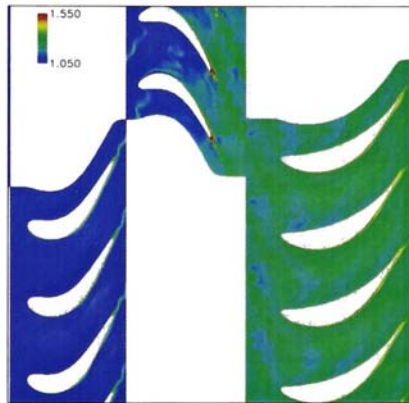


Figure 11.4: Nozzle 2 - Nozzle 3 Instantaneous Entropy Contours - High Efficiency.

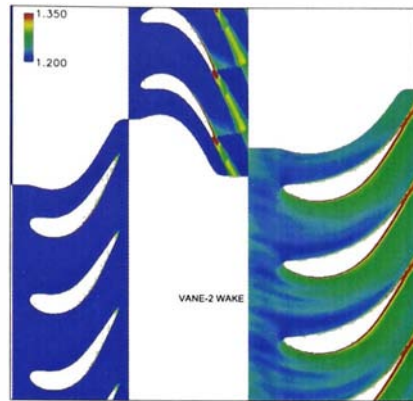


Figure 11.5: Nozzle 2 - Nozzle 3 Time-Averaged Entropy Contours - Low Efficiency.

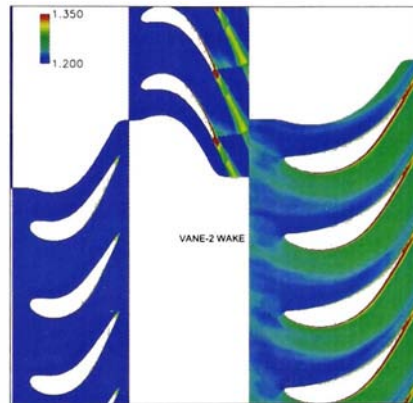


Figure 11.6: Nozzle 2 - Nozzle 3 Time-Averaged Entropy Contours - High Efficiency.

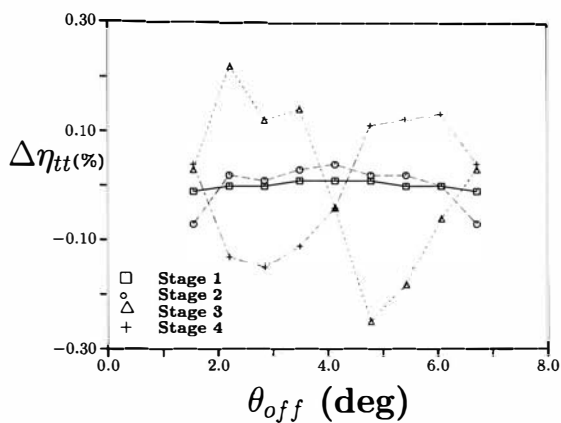


Figure 11.7: Stage Efficiencies.

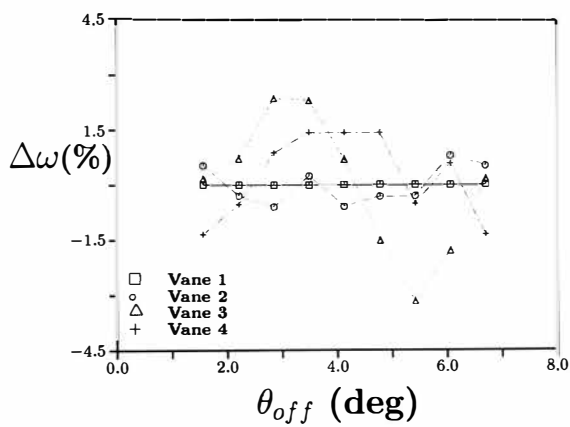


Figure 11.8: Vane Losses With Respect to Vane 3 Clocking Position.

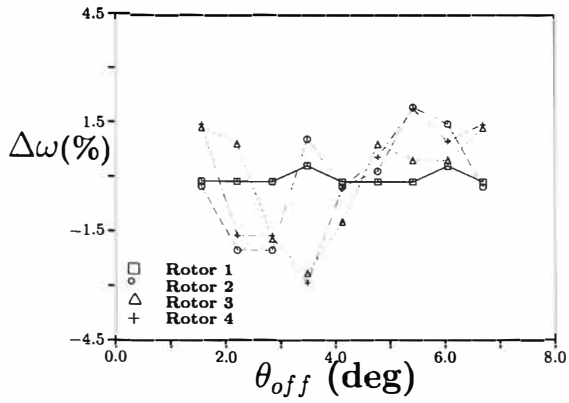


Figure 11.9: Rotor Losses With Respect to Vane 3 Clocking Position.

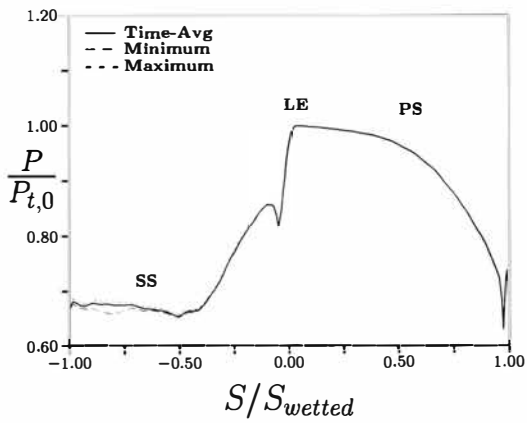


Figure 11.10: Unsteady Pressure Envelopes - Vane 1.

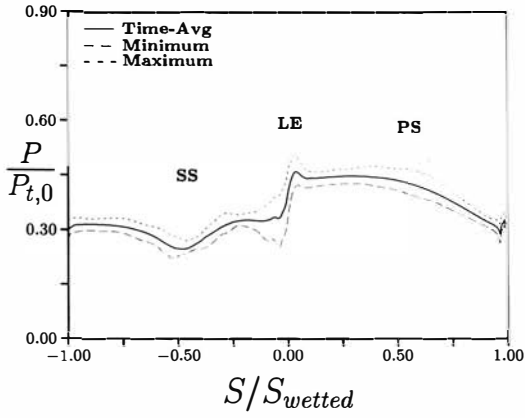


Figure 11.11: Unsteady Pressure Envelopes - Vane 2.

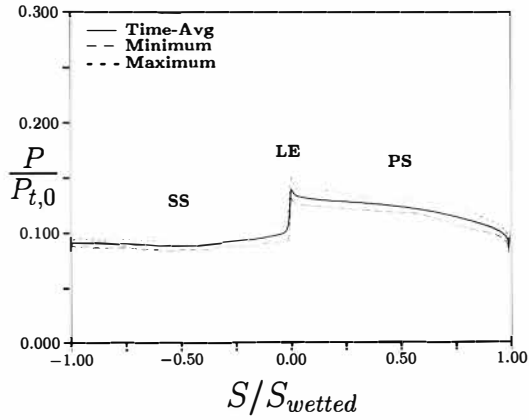


Figure 11.12: Unsteady Pressure Envelopes - Vane 3.

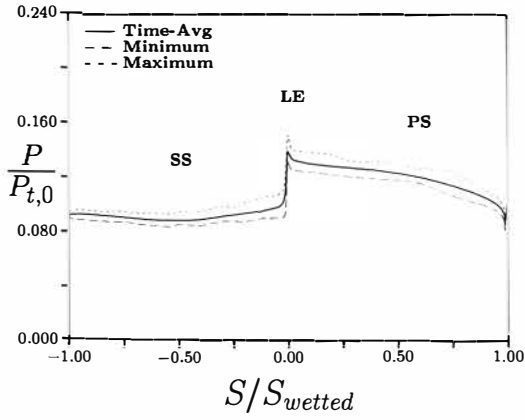


Figure 11.13: Unsteady Pressure Envelopes - Vane 4.

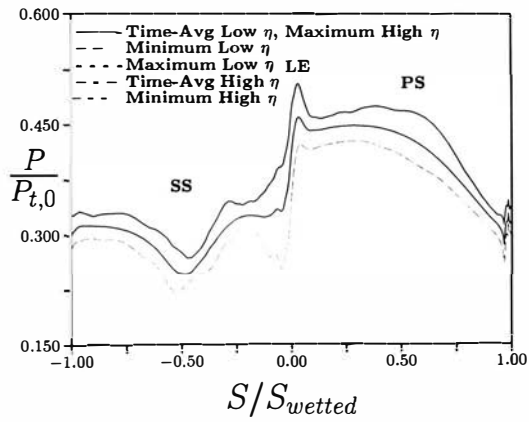


Figure 11.14: Maximum and Minimum Unsteady Pressure Envelopes - Vane 2.

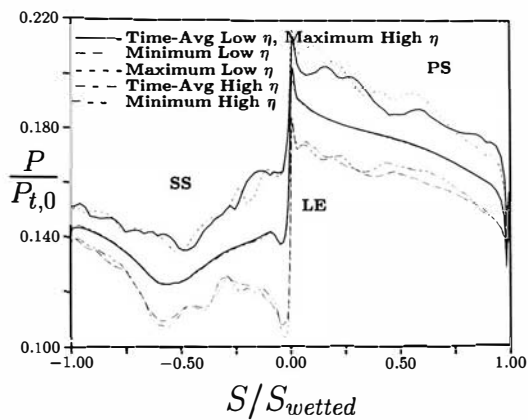


Figure 11.15: Maximum and Minimum Unsteady Pressure Envelopes - Vane 3.

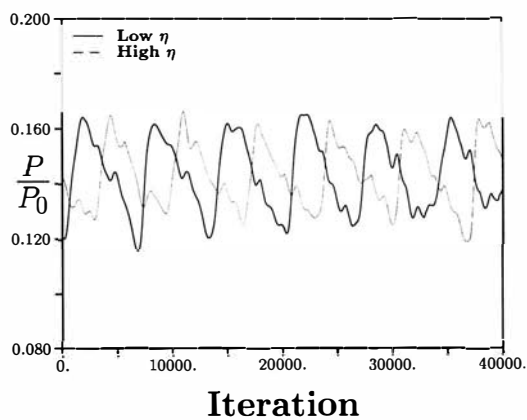


Figure 11.16: Maximum and Minimum Unsteady Pressure Histories - Vane 3 Leading Edge.

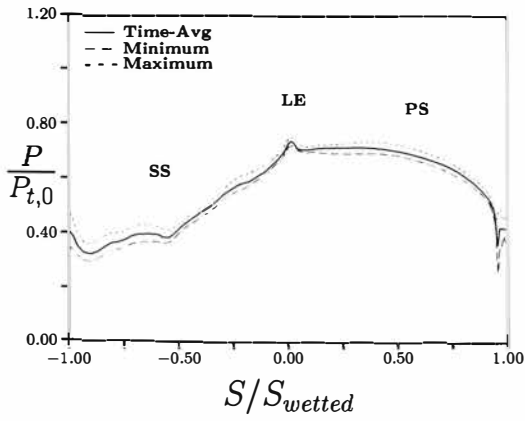


Figure 11.17: Unsteady Pressure Envelopes - Rotor 1.

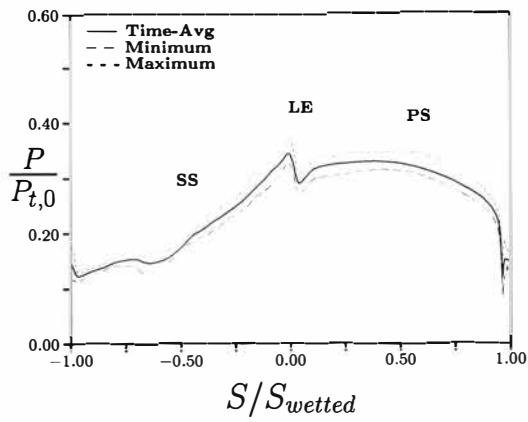


Figure 11.18: Unsteady Pressure Envelopes - Rotor 2.

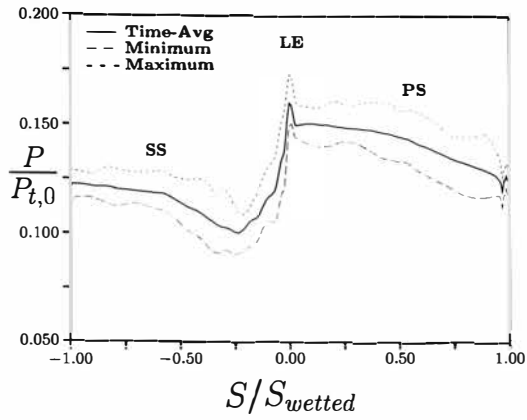


Figure 11.19: Unsteady Pressure Envelopes - Rotor 3.

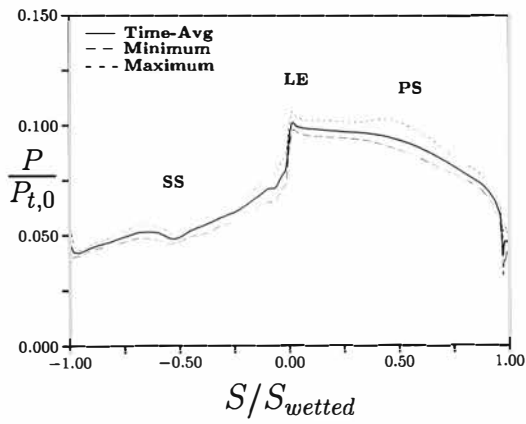


Figure 11.20: Unsteady Pressure Envelopes - Rotor 4.

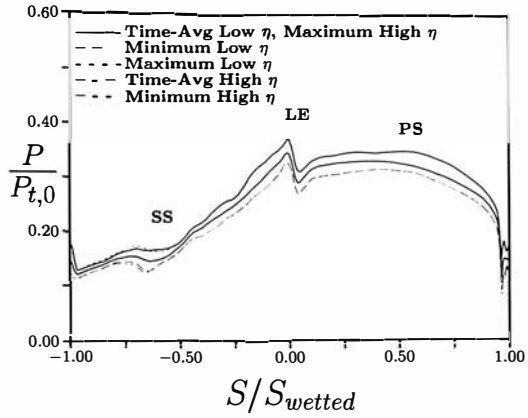


Figure 11.21: Maximum and Minimum Unsteady Pressure Envelopes - Rotor 2.

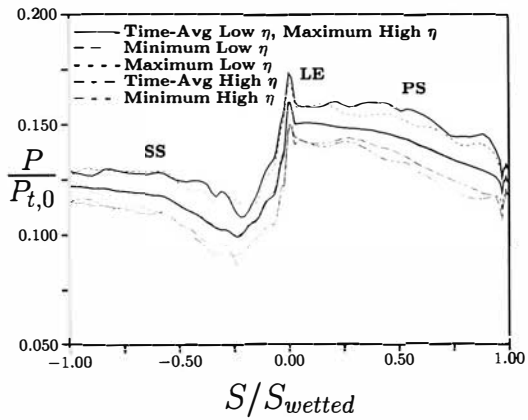


Figure 11.22: Maximum and Minimum Unsteady Pressure Envelopes - Rotor 3.

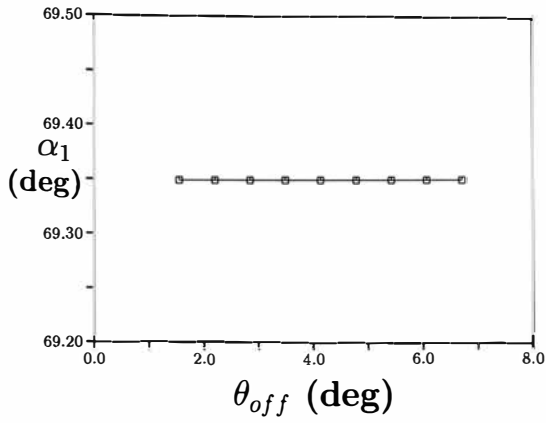


Figure 11.23: Time-Averaged Absolute Exit Flow Angle - Nozzle 1.

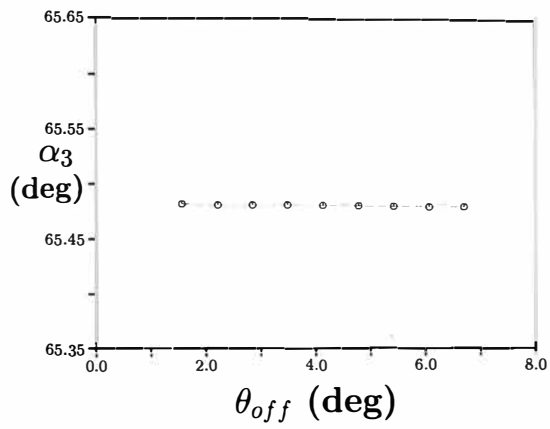


Figure 11.24: Time-Averaged Absolute Exit Flow Angle - Nozzle 2.

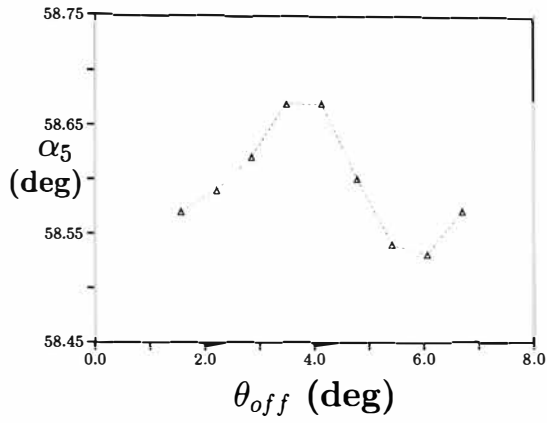


Figure 11.25: Time-Averaged Absolute Exit Flow Angle - Nozzle 3.

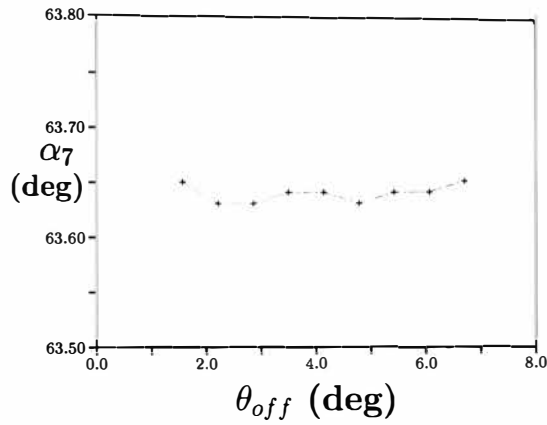


Figure 11.26: Time-Averaged Absolute Exit Flow Angle - Nozzle 4.

CHAPTER 12 Conclusions

A numerical study has been completed taking into consideration hot streak frequency effects on propagation and mid-span heat transfer. Results indicate grid density is a governing factor in time-accurate simulation of temporal fluctuations requiring a fine grid spacing to properly capture the combined effects of spatial and temporal variational flow physics. Rotor surface temperatures are not substantially affected by hot streak frequencies less than unity, showing maximum temperature differences on the order of 1.2% for both the pressure and suction surfaces. Stator 2 time-averaged surface profiles are observed to be heavily dependent upon hot streak frequency and its effect on rotor exit temperature profiles. Oscillations at unity provide a particularly unique case for rotor loading studies since at this frequency the hot streak can be made to impact anywhere from the leading edge to the trailing edge of the pressure surface based on the phase shifting applied to the equation. Phase shifting the hot streak has inverse effects on the rotor and stator. For example, for the nominal, unlocked case the rotor loading is the inverse of the second stator. Clocking the second stage is also a useful property, not only with respect to the first-stage stator but also with respect to the hot streak for cases with a hot streak introduced at mid-span. This is a more classical clocking procedure, instead of repositioning the hot streak to impact the leading edge of the first-stage stator. Since it is much easier to implement cooling schemes on non-rotating blade rows as opposed to rotating rows, a combination of clocking and frequency manipulation can be used to alleviate the

thermal loading on the rotor, and place it on the second stator. This can pull much of the wasted mass flow from costly inefficient rotor cooling and be more effectively used on the stator, increasing overall efficiency.

Additionally, a performance study has been completed for airfoil clocking of an embedded stage in a four-stage axial turbine. Clocking results show time periodicity effects produced by clocking in both efficiency and loss for the clocked blade row as well as downstream bladerows. Unsteadiness is observed to increase when efficiency is at a maximum, and decrease when efficiency is at a minimum. Rotor loss is observed to vary inversely to vane loss, though reaching greater magnitudes at both maximum and minimum than does the vane. Variations aft of the clocked row are observed to vary inversely to that of the clocked row (*i.e.* rotor losses in the aft rows are the inverse of the clocked row.) Efficiency maximums and minimums are shown to agree with previous studies, reaching a maximum when the upstream wake impinges the leading edge of the clocked airfoil, and a minimum when the wake passes in the mid-passage region. Entropy and vortex generation is shown to increase with axial distance through the machine.

Hot streak temporal migration trends offer especially tempting prospects to design engineers and combustor control engineers. Designing pulsating trends such as this into current combustion processes could provide a means to increase work output and efficiency by allowing for more efficient usage of mass flow. Internal stage clocking offers propagational effects to multi-stage turbomachines, such that by clocking one internal row, others can be staggered from it to achieve an even higher total efficiency.

BIBLIOGRAPHY

- [1] Butler, T. L., Sharma, O. P., Joslyn, H. D., Dring, R. P. "Redistribution of an Inlet Temperature Distortion in an Axial Flow Turbine Stage", *Journal of Propulsion and Power*, Vol. 5, No. 1, 1989, pp. 64-71.1986.
- [2] Sharma, O. P., Dorney, D. J., Tanikrut, S. Ni, R. H., "Turbine Flows: The Impact of Unsteadiness," Applied Computational Fluid Dynamics, New York, 1998.
- [3] Kerrebrock, J. L, and Mikolajczak, A. A., "Intra-Stator Transport of Rotor Wakes and its Effect on Compressor Performance," *ASME Journal of Engineering and Power*, Vol. 92, Oct. 1970, pp. 359-369.
- [4] Rodback, R., and Dring, R. P., "Turbine Heat Transfer Research- Hot Streaks and Phantom Cooling. Part 1 - Separate Effects.", 1992.
- [5] Roback, R., and Dring, R. P., "Turbine Heat Transfer Research- Hot Streaks and Phantom Cooling. Part 2 - Combined Effects and Analytical Modeling", 1992.
- [6] Schwab, J. R. and Stabe, R. G., "Analytical and Experimental Study of Flow Through an Axial Turbine With a Nonuniform Inlet Radial Temperature Profile", AIAA Paper 83-1175, 1983.
- [7] Dorney, Daniel J., and Schwab, J. R., 1995, "Unsteady Numerical Simulations of Radial Temperature Profile Redistribution in a Single Stage Turbine", ASME Paper 95-GT-178, 1995.
- [8] Dorney, D. J., and Gundy-Burlet, K. L., "Effects of Hot Streak Shape on Rotor Heating in a High-Subsonic Single-Stage Turbine," ASME Paper 2000-GT-0449, Presented at ASME Turbo Expo 8-11 May 2000, Munich, Germany.
- [9] Gundy-Burlet, Karen L. and Dorney, Daniel J., "Three-Dimensional Simulations of Hot Streak Clocking in a 1-1/2 Stage Turbine", 32nd Joint Propulsion Conference, July 1-3, 1996.
- [10] Takahashi R. K., Ni, R. H., Sharma, O. P., and Staubach, J. B., "Effects of Hot Streak Clocking in a 1-1/2 Stage Turbine," AIAA Paper 96-2796, 32nd Joint Propulsion Conference, July 1-3, 1996.
- [11] Takahashi, R. K., NI, R. H., "Unsteady Euler Analysis of the Redistribution of an Inlet Temperature Distortion in a Turbine", 26th Joint Propulsion Conference, July, 1990.
- [12] Takahashi, R. K., Ni R. H., "Unsteady Hot Streak Simulation Through a 1-1/2 Stage Turbine", AIAA Paper 91-3382, 1991.

- [13] Dorney, D. J., Ng, B., Al-Habbas, A., Gundy-Burlet, K. "Numerical Simulations of Hot Streak Migration in a 1-1/2 Stage Turbine," AIAA Paper 95-0181, 33rd Aerospace Meeting and Exhibit, January, 1995.
- [14] Dorney, Daniel J., Gundy-Burlet, Karen L., Sondak, Douglas L., "A Survey of Hot Streak Simulations", *International Journal of Turbo and Jet Engines*, Vol. 16, January 1999.
- [15] Rai, M. M., Dring, R. P. "Navier-Stokes Analysis of the Redistribution of Inlet Temperature Distortion in a Turbine", 23rd Joint Propulsion Conference. June 29- July, 1987.
- [16] Shang, T. Epstein, A. H., "Analysis of Hot Streak Effects on a Turbine Rotor Heat Load," Presented at the International Gas Turbine and Aeroengine Congress and Exhibition, June, 1996.
- [17] Dorney, Daniel J., Davis, R. L., Edwards, D. E., Madavan, N. K., "Unsteady Analysis of Hot Streak Migration in a Turbine Stage" *Journal of Propulsion and Power*, Vol. 8, No. 2, 1992, pp. 520-529
- [18] Dorney, D. J., and Gundy-Burlet, K. L., "Effects of Radial Location on the Migration of Hot Streaks in a Turbine," *Journal of Propulsion and Power*, Vol. 16, No. 3, 2000, pp. 377-387.
- [19] Johnston, R. T. and Fleeter, Sanford, "Airfoil Wake Interactions in a High Speed Axial Compressor," AIAA Paper 96-2821, 32nd Joint Propulsion Conference, July 1996.
- [20] Giles, M. B., "Calculation of Unsteady Wake/Rotor Interactions," AIAA Paper 87-0006, 25th AIAA Aerospace Sciences Meeting, January, 1987.
- [21] Gundy-Burlet, K. L. and Dorney, D. J., "Investigations of Airfoil Colcking and Inter-Blade-Row Gaps in Axial Compressors," AIAA Paper 97-3008, 33rd Joint Propulsion Conference and Exhibit, June 1997.
- [22] Saren, V. E., Savin, N. M., Dorney, D. J., Sondak, D. L., "Experimental and Numerical Investigation of Airfoifl Clocking and Inter-Blade-Row Gap Effects in Axial Compressor Performance," *International Journal of Turbo and Jet Engines*, Vol. 15, pp. 325-252, 1998.
- [23] Dorney, D. J., Sondak, D. L., Cizmas, P. G. A., Saren, V. E., Savin, N. M., "Full-Annulus Simulations of Airfoil Clocking in a Compressor at Off-Design Operating Conditions," *International Journal of Turbo and Jet Engines*, Vol. 17, pp. 95-117, 2000.
- [24] Dorney, D. J., Merz, L. F., Sondak, D. L., Damle, S. V., Stringham, J., "Performance Increases in an Industrial Compressor Through Airfoil Clocking," AIAA Paper 2001-0527, 39th Aerospace Sciences Meeting & Exhibit, 8-11 January 2001 / Reno, NV.
- [25] Dorney, D. J., Sharma, O. P., "Turbine Performance Increases Through Airfoil Clocking," *International Journal of Turbo and Jet Engines*, Vol. 15, pp. 119-127, 1998.

- [26] Cizmas, P., Dorney, D., "Parallel Computaion of Turbine Blade Clocking," *International Journal of Turbo and Jet Engines*, Vol. 16, pp. 49-60, 1999.
- [27] Dorney, D. J., Sondak, D. L., "Three-Dimensional Simulations of Airfoil Clocking in a 1-1/2 Stage Turbine" AIAA Paper 2000-3359, 36th Joint Propulsion Conference and Exhibit, July, 2000.
- [28] Huber, F. W., Johnson, P. D., Sharma, O. P., Staubach, J. B., and Gaddis, S. W., "Performance Improvement Through indexing of Turbine Airfoils: Part 1 - Experimental Investigation," *ASME Journal of Turbomachinery*, Vol. 118, pp. 630-635, Oct. 1996.
- [29] Griffin, L. W., Huber, F. W., and Sharma, O. P., "Performance Improvement Through indexing of Turbine Airfoils: Part 2 - Numerical Simulation," *ASME Journal of Turbomachinery*, Vol. 118, pp. 636-642, Oct. 1996.
- [30] Baldwin, B. S., and Lomax, H., "Thin Layer Approximation And Algebraic Model For Separated Flow," AIAA Paper 78-257, January 1978.
- [31] Dorney, Daniel J., Davis, Roger L., Sharma, Om P., "Two Dimensional Inlet Temperature Profile Alteration in a Turbine Stage", ASME Paper 91-GT-406, 36th ASME International Gas Turbine and Aeroengine Congress and Exposition, June, 1991.
- [32] Rai, M. M. and Madavan, N. K., "Multi-Airfoil Navier-Stokes Simulations of Turbine Rotor/Stator Interaction," AIAA Paper 88-0361, 26th Aerospace Sciences Meeting, January 1988.
- [33] Ryder, R. *Private Communication*, Conducted by Dorney, D. J., June, 1998.
- [34] Krouthen B., and Giles, M., "Numerical Investigation of Hot Streaks in Turbines," AIAA Paper 88-3015, July 1988.

VITA